HYDRODYNAMIC EFFECT OF EARTHQUAKES ON CIRCULAR DAM-RESERVOIR SYSTEMS

by

D. S. Kadle and Allen T. Chwang

Sponsored by

National Science Foundation
Grants ENG 79-10049 and CME 80-20564

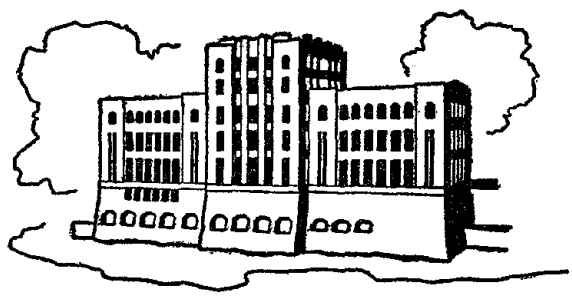

IIHR Report No. 246

Iowa Institute of Hydraulic Research
The University of Iowa
Iowa City, Iowa 52242

August 1982

HYDRODYNAMIC EFFECT OF EARTHQUAKES ON CIRCULAR DAM-RESERVOIR SYSTEMS

by

D. S. Kadle and Allen T. Chwang

Sponsored by

National Science Foundation
Grants ENG 79-10049 and CME 80-20564

IIHR Report No. 246

Iowa Institute of Hydraulic Research
The University of Iowa
Iowa City, Iowa 52242

August 1982

ABSTRACT

This report represents essentially the thesis submitted by D.S. Kadle in partial fulfillment of the requirements for the degree of Master of Science in Mechanical Engineering at The University of Iowa. Professor Allen T. Chwang was supervisor of the research project and thesis advisor.

The present study deals with the hydrodynamic effect of earthquakes on a three-dimensional dam-reservoir system. Analytical solutions in closed forms have been obtained when the reservoir is circular or semi-circular in shape. The effects of surface waves and compressibility of the fluid in the reservoir have also been included. In the case of no surface waves, it was found that the in-phase component of the hydrodynamic pressure increases with the depth of the reservoir and attains a maximum value at the base of the dam. In the presence of surface waves, the in-phase component was slightly reduced for small values of the wave-effect parameter C. However, for large values of C, the pressure distribution was found to be oscillatory. Resonances were found to occur when the ratio of the fluid depth to the period of the ground motion was greater than 360 m/sec.

TABLE OF CONTENTS

LIST OF FIGURES

LIST OF SYMBOLS

a	amplitude of the ground acceleration
B	dimensionless compressibility parameter $\omega h/c_o$
C	dimensionless wave-effect parameter $g/(\omega^2 h)$
c_o	constant velocity of sound in undisturbed water
C_F	dimensionless force coefficient for circular reservoir
C_{Fl}	total dimensionless force coefficient for semi-circular reservoir
C_{Fi}	in-phase component of the dimensionless force coefficient for semi-circular reservoir
C_M	dimensionless moment coefficient for circular reservoir
C_{Ml}	total dimensionless moment coefficient for semi-circular reservoir
C_{Mi}	in-phase component of dimensionless moment coefficient for semi-circular reservoir
C_p	dimensionless pressure coefficient for circular reservoir
C_{pl}	total dimensionless pressure coefficient for semi-circular reservoir
C_{pi}	in-phase component of the dimensionless pressure coefficient for semi-circular reservoir
E_ν	Weber function of order ν
g	acceleration due to gravity
h	constant depth of reservoir
H	height of dam
I_n	modified Bessel function of first kind, of order n

J_n Bessel function of first kind, of order n

ℓ width of dam

M largest integer for which $\frac{\omega}{c_o} \geq \lambda_m$

P hydrodynamic pressure

P_o $\sinh \lambda_o h$

P_m $\sin \lambda_m h$

Q_o $\cosh \lambda_o h$

Q_m $\cos \lambda_m h$

r radial distance

R radius of the reservoir

t time

T period of ground motion

α phase difference between the in-phase and out-of-phase components of the pressure coefficient C_{p1} in the semi-circular reservoir

β phase difference between the in-phase and out-of-phase components of the force coefficient C_{F1} in the semi-circular reservoir

γ phase difference between the in-phase and out-of-phase components of the moment coefficient C_{M1} in the semi-circular reservoir

η wave elevation with respect to undisturbed free surface

θ_o half-angle subtended by the dam at the center of the circular reservoir

λ_o root of $C\ \lambda_o h\ \tanh \lambda_o h - 1 = 0$

λ_m roots of $C\ \lambda_m h\ \tan \lambda_m h + 1 = 0$

μ_o $\sqrt{\lambda_o^2 + (\frac{\omega}{c_o})^2}$

$\mu_m \sqrt{(\frac{\omega}{c_o})^2 - \lambda_m^2}$

ρ density of water

ρ_o constant density of undisturbed water

ϕ velocity potential

ω frequency of ground motion

$*$ superscript denotes dimensionless variables non-dimensionalized by the depth of the reservoir h

I. INTRODUCTION

1.1 Review of Pertinent Literature

The hydrodynamic pressures developed during earthquakes play an important role in the design of dams. During an earthquake, the dam accelerates into and away from the reservoir, developing a hydrodynamic pressure in excess of the hydrostatic pressure. Depending on the intensity of an earthquake, this pressure could be large enough to cause a dam to collapse and have calamitous consequences on a dense population downstream of the dam. The present work deals with some aspects of this problem.

The pioneering work in this field was conducted by Westergaard (1933). He derived an expression for the hydrodynamic pressure exerted on the vertical upstream face of a rigid, infinitely long dam, as a result of horizontal ground motion. He also introduced the "added mass" concept. A simple momentum-balance method was presented by von Kármán (1933) who obtained a distribution of the "added mass" and consequently the hydrodynamic pressure along the upstream face of a rigid dam. However, the Westergaard solution is valid only for harmonic excitations greater than the fundamental natural frequency of the reservoir (Kotsubo, 1959).

The hydrodynamic pressures developed on dams whose upstream face is not vertical was determined experimentally using an electrical analogue (Zangar and Haefeli, 1952; Zangar, 1953). Von Kármán's

momentum-balance method was adopted by Chwang and Housner (1978) to investigate the earthquake forces on a rigid dam having an inclined upstream face of constant slope. They concluded that the hydrodynamic pressure, at any given height, increases with an increase in the slope of the dam; the maximum value being attained for a vertical dam. Later, Chwang (1978) approached the same problem by using a two-dimensional potential-flow theory and found a reasonable agreement with the momentum-balance method.

The effect of compressibility of fluid has received considerable attention. While many authors (Westergaard, 1933; von Kármán, 1933; Chwang, 1978) have assumed the fluid to be incompressible, some authors have taken into consideration the compressibility of the fluid (Chopra, 1967; Kotsubo, 1959; Huang 1980). It was found (Chopra, 1967) that the compressibility effect becomes important if excitation frequency is very high.

The problem of finite reservoirs has been analyzed by Werner and Sundquist (1949) and Huang (1980). This problem was also solved by Chwang (1979) who found that for horizontal accelerations, the pressure reduces as the reservoir becomes smaller in size. He also found that the effect of vertical acceleration is to adjust the hydrostatic pressure by using an effective gravitational constant and this is true for arbitrary shaped reservoirs. The possibility of cavitation was also explored in Chwang's (1979) paper.

1.2 Assumptions

Essentially, the problem of hydrodynamic effect of earthquakes on a dam-reservoir system can be divided into three broad categories:

(1) Response of the dam to earthquakes neglecting the hydrodynamic effects;

(2) Hydrodynamic effects of earthquakes on a rigid dam;

(3) Hydrodynamic effects of earthquakes on a flexible dam, which considers the interaction of the first two problems.

The present work is concerned with the second problem for a circular and a semi-circular reservoir. These two problems are the extreme cases for reservoirs having the shape of a sector of a circle (see Fig. 1). The Hiwassee dam-reservoir complex of the Tennessee Valley Authority is approximately circular. The hydrodynamic pressure will be the real part of the complex pressure due to horizontal acceleration $a\, e^{i\omega t}$ in the x direction.

The assumptions made are that the fluid is compressible and inviscid and that the flow is irrotational with the presence of surface waves. The dam and reservoir walls are assumed to be vertical and rigid. The amplitude of the excitation is assumed to be small. In this thesis, the effect of the wave-effect parameter, the compressibility of the water and the dimensions of the dam on the hydrodynamic pressure will be discussed in detail and presented graphically for longitudinal excitations.

II. CIRCULAR RESERVOIR-DAM SYSTEM

2.1 Governing Equations and Boundary Conditions

The dam-reservoir system under consideration is one in which the reservoir is approximately circular in shape with constant depth h and radius R. The dam height is H and the width is ℓ. The origin is located at the center of the base of the dam. The x-axis is in a direction perpendicular to the downstream face of the dam and lies in the horizontal ground plane. The y-axis is perpendicular to the x-axis in the horizontal plane. The z-axis points vertically upwards. The radial distance r is measured from the center of reservoir, as is the angle θ (see Fig. 2). Thus,

$$x = r\cos\theta - R\cos\theta_o , \qquad y = r\sin\theta .$$

It is assumed that the ground acceleration is $-ae^{i\omega t}$ along the positive x direction and that there is no attenuation.

For irrotational motions of an inviscid, compressible fluid, the velocity vector has a scalar potential ϕ. The effect of an earthquake on this dam-reservoir system is to create a pressure wave which, under the assumption of small amplitudes, is governed by a linearized wave equation

$$\nabla^2 p = \frac{1}{c_o^2}\,\frac{\partial^2 p}{\partial t^2} , \tag{2.1}$$

where ∇^2 is the Laplacian operator in the cylindrical polar co-ordinate system (r,θ, z) and c_o is the constant velocity of sound in undisturbed water given by

$$c_o = \sqrt{\left(\frac{\partial P}{\partial \rho}\right)_s} \ . \tag{2.2}$$

Here c_o has been evaluated at constant entropy s and ρ is the density of water. In the linearized theory of wave propagation, the hydrodynamic pressure P is related to the velocity potential ϕ by

$$P = - \rho_o \frac{\partial \phi}{\partial t} \ , \tag{2.3}$$

where ρ_o is the constant density of undisturbed water. Thus, by (2.1) and (2.3), the velocity potential ϕ also satisfies the wave equation (2.1),

$$\nabla^2 \phi = \frac{1}{c_o^2} \frac{\partial^2 \phi}{\partial t^2} \ . \tag{2.4}$$

The boundary conditions for ϕ are as follows:

(i) zero normal velocity at the bottom of the reservoir,

$$\frac{\partial \phi}{\partial z} (r,\theta,0,t) = 0 \ ; \tag{2.5}$$

(ii) condition of symmetry,

$$\frac{\partial \phi}{\partial \theta} (r,0,z,t) = \frac{\partial \phi}{\partial \theta} (r,\pi,z,t) = 0 \ ; \tag{2.6}$$

(iii) The linearized kinematic boundary condition at the free surface (see Fig. 3),

$$\frac{\partial \phi}{\partial z} = \frac{\partial \eta}{\partial t} \quad \text{at} \quad z = h \; ; \tag{2.7}$$

(iv) The linearized dynamic boundary condition at the free surface,

$$\frac{\partial \phi}{\partial t} + g\eta = 0 \quad \text{at} \quad z = h \; . \tag{2.8}$$

Combining (2.7) and (2.8), we get the free surface boundary condition,

$$\frac{\partial^2 \phi}{\partial t^2} + g \frac{\partial \phi}{\partial z} = 0 \quad \text{at} \quad z = h \; . \tag{2.9}$$

(v) This boundary condition is on the dam surface where

$$r = \frac{R \cos \theta_o}{\cos \theta} , \qquad |\theta| \leq |\theta_o| \; . \tag{2.10}$$

If the width of the dam is very small in comparison with the radius of the reservoir, $\ell/R << 1$, equation (2.10) reduces to

$$r = R[1 + O\left(\frac{\ell}{R}\right)^2] , \quad \theta = O(\ell/R) \tag{2.11}$$

and since

$$\frac{\partial \phi}{\partial x} = \frac{\partial \phi}{\partial r} \cos\theta - \frac{\sin\theta}{r} \frac{\partial \phi}{\partial \theta} = \frac{\partial \phi}{\partial r} + O(\ell/R)$$

then the boundary condition on the rigid dam surface and reservoir may be approximated by

$$\frac{\partial \phi}{\partial r}(R,\theta,z,t) = \frac{i}{\omega} a e^{i\omega t} \cos\theta \ . \tag{2.12}$$

2.2 Velocity Potential and Pressure Distribution

Solving (2.4) subject to the boundary conditions (2.5), (2.6), (2.9) and (2.12), we obtain (see Appendix A)

$$\phi(r,\theta,z,t) = \frac{4ia\cos\theta}{\omega h} e^{i\omega t} \left\{ \frac{P_o \cosh \lambda_o z \, J_1(\mu_o r)}{\lambda_o \mu_o (1 + CP_o^2)[J_o(\mu_o R) - J_2(\mu_o R)]} \right.$$

$$+ \sum_{m=1}^{M} \frac{P_m \cos \lambda_m z \, J_1(\mu_m r)}{\lambda_m \mu_m (1 - CP_m^2)[J_o(\mu_m R) - J_2(\mu_m R)]}$$

$$\left. + \sum_{m=M+1}^{\infty} \frac{P_m \cos\lambda_m z \, I_1(\beta_m r)}{\lambda_m \beta_m (1 - CP_m^2)[I_o(\beta_m R) + I_2(\beta_m R)]} \right\}, \tag{2.13}$$

where λ_o satisfies

$$C\lambda_o h \tanh \lambda_o h - 1 = 0 \ , \tag{2.14}$$

λ_m satisfies

$$C\lambda_m h \tan\lambda_m h + 1 = 0 \quad (m = 1,2,3\ldots) \ , \tag{2.15}$$

$$P_o = \sinh \lambda_o h \ , \tag{2.16}$$

$$P_m = \sin \lambda_m h \qquad (m = 1,2,3\ldots) \ , \tag{2.17}$$

$$\mu_o = \sqrt{\lambda_o^2 + \left(\frac{\omega}{c_o}\right)^2} \quad , \tag{2.18}$$

$$\mu_m = \sqrt{\left(\frac{\omega}{c_o}\right)^2 - \lambda_m^2} \qquad (m = 1,2,3,\ldots,M) \ , \tag{2.19}$$

$$\beta_m = \sqrt{\lambda_m^2 - \left(\frac{\omega}{c_o}\right)^2} \qquad (m = M+1,\ M+2,\ldots) \ , \tag{2.20}$$

M is the largest integer for which $\frac{\omega}{c_o} \geq \lambda_m$, and the wave-effect parameter C is given by

$$C = \frac{g}{\omega^2 h} \ . \tag{2.21}$$

In equation (2.13), $J_n(x)$ denotes the Bessel function of the first kind, of order n, and $I_n(x)$ denotes the modified Bessel function of the first kind, of order n.

It should be noted that (2.14) and (2.21) give the usual dispersion relation for surface waves,

$$\omega^2 = g\lambda_o \tanh \lambda_o h \ . \tag{2.22}$$

Since the frequency of the ground excitation ω is given, equation (2.22) uniquely determines the wave number λ_o and consequently the wavelength of the surface wave produced by the vibration of the dam.

Neglecting terms of the order (ℓ/R), the hydrodynamic pressure on the upstream face of the dam is obtained from (2.3) and (2.13) as the

real part of $-\rho_o \left.\frac{\partial \phi}{\partial t}\right|_{r=R,\theta=0}$. Therefore,

$$P = \frac{4\rho_o a}{h} \cos\omega t \left\{ \frac{P_o \cosh \lambda_o z \, J_1(\mu_o R)}{\lambda_o \mu_o (1 + CP_o^2)[J_o(\mu_o R) - J_2(\mu_o R)]} \right.$$

$$+ \sum_{m=1}^{M} \frac{P_m \cos\lambda_m z \, J_1(\mu_m R)}{\lambda_m \mu_m (1 - CP_m^2)\,[J_o(\mu_m R) - J_2(\mu_m R)]}$$

$$\left. + \sum_{m=M+1}^{\infty} \frac{P_m \cos \lambda_m z \, I_1(\beta_m R)}{\lambda_m \beta_m (1 - CP_m^2)[I_o(\beta_m R) + I_2(\beta_m R)]} \right\} . \qquad (2.23)$$

Defining the dimensionless pressure coefficient C_p by

$$\frac{P(R,0,z,t)}{\rho_o a h} = C_p \cos \omega t \, , \qquad (2.24)$$

we obtain

$$C_p = 4 \left\{ \frac{P_o \cosh \lambda_o^* z^* J_1(\mu_o^* R^*)}{\lambda_o^* \mu_o^* (1 + CP_o^2)[J_o(\mu_o^* R^*) - J_2(\mu_o^* R^*)]} \right.$$

$$+ \sum_{m=1}^{M} \frac{P_m \cos \lambda_m^* z^* J_1(\mu_m^* R^*)}{\lambda_m^* \mu_m^* (1 - CP_m^2)[J_o(\mu_m^* R^*) - J_2(\mu_m^* R^*)]}$$

$$\left. + \sum_{m=M+1}^{\infty} \frac{P_m \cos \lambda_m^* z^* I_1(\beta_m^* R^*)}{\lambda_m^* \beta_m^* (1 - CP_m^2)[I_o(\beta_m^* R^*) + I_2(\beta_m^* R^*)]} \right\} , \qquad (2.25)$$

where

$$\lambda_o^* = \lambda_o h, \quad \lambda_m^* = \lambda_m h \quad (m = 1,2,\ldots) , \tag{2.26a}$$

$$\mu_o^* = \mu_o h , \quad \mu_m^* = \mu_m h, \quad \beta_m^* = \beta_m h \quad (m = 1,2,\ldots) , \tag{2.26b}$$

and

$$R^* = R/h , \quad z^* = z/h . \tag{2.26c}$$

If we define a dimensionless compressibility parameter B by

$$B = \frac{\omega h}{c_o} , \tag{2.27}$$

then

$$\mu_o^* = \sqrt{B^2 + \lambda_o^{*2}} , \tag{2.28a}$$

$$\mu_m^* = \sqrt{B^2 - \lambda_m^{*2}} \quad (m = 1,2,\ldots,M) , \tag{2.28b}$$

and

$$\beta_m^* = \sqrt{\lambda_m^{*2} - B^2} \quad (m = M+1, M+2,\ldots) . \tag{2.28c}$$

An incompressible fluid requires B = 0.

2.3 Hydrodynamic Force and Moment Coefficients

The hydrodynamic force coefficient C_F at the dam surface per unit width can be obtained from

$$C_F = \frac{1}{h}\int_0^h C_P \, dz \ . \tag{2.29}$$

Thus,

$$C_F = 4\left\{\frac{P_o^2 \, J_1(\mu_o^* R^*)}{\lambda_o^{*2}\mu_o^*(1 + CP_o^2)[J_o(\mu_o^* R^*) - J_2(\mu_o^* R^*)]}\right.$$

$$+ \sum_{m=1}^{M} \frac{P_m^2 \, J_1(\mu_m^* R^*)}{\lambda_m^{*2}\mu_m^*(1 - CP_m^2)[J_o(\mu_m^* R^*) - J_2(\mu_m^* R^*)]}$$

$$\left. + \sum_{m=M+1}^{\infty} \frac{P_m^2 \, I_1(\beta_m^* R^*)}{\lambda_m^{*2}\beta_m^*(1 - CP_m^2)[I_o(\beta_m^* R^*) + I_2(\beta_m^* R^*)]}\right\} \ . \tag{2.30}$$

The hydrodynamic moment coefficient C_M at the dam surface with respect to its base can be obtained from

$$C_M = \frac{1}{h^2}\int_0^h z C_p \, dz \ . \tag{2.31}$$

Thus,

$$C_M = 4\left\{ \frac{P_o(\lambda_o^* P_o - Q_o + 1)\, J_1(\mu_o^* R^*)}{\lambda_o^{*3}\mu_o^*(1 + CP_o^2)[J_o(\mu_o^* R^*) - J_2(\mu_o^* R^*)]} \right.$$

$$+ \sum_{m=1}^{M} \frac{P_m(\lambda_m^* P_m + Q_m - 1)\, J_1(\mu_m^* R^*)}{\lambda_m^{*3}\mu_m^*(1 - CP_m^2)[J_o(\mu_m^* R^*) - J_2(\mu_m^* R^*)]}$$

$$\left. + \sum_{m=M+1}^{\infty} \frac{P_m(\lambda_m^* P_m + Q_m - 1)\, I_1(\beta_m^* R^*)}{\lambda_m^{*3}\beta_m^*(1 - CP_m^2)[I_o(\beta_m^* R^*) + I_2(\beta_m^* R^*)]} \right\}, \qquad (2.32)$$

where

$$Q_o = \cosh \lambda_o h \ , \qquad (2.33)$$

$$Q_m = \cos \lambda_m h \quad (m = 1,2,\ldots) \ , \qquad (2.34)$$

and other dimensionless parameters $\lambda_o^*, \lambda_m^*, \mu_o^*, \mu_m^*, \beta_m^*$, R^*, P_o and P_m have been defined in equations (2.26), (2.16) and (2.17).

III. SEMI-CIRCULAR RESERVOIR-DAM SYSTEM

3.1 Governing Equations and Boundary Conditions

In this chapter, the reservoir will be assumed to be semi-circular in shape with constant depth h and radius R. The dimensions of the dam are its height H and its width ℓ(ℓ = 2R). The origin is located at the center of the base of the dam. The x-axis is in a direction perpendicular to the upstream face of the dam and lies in the horizontal ground plane. The y-axis is perpendicular to the x-axis in the horizontal plane and the z-axis points vertically upwards. The radial distance r is measured from the origin 0 as is the angle θ (See Fig. 4). It is assumed that the ground acceleration is $ae^{i\omega t}$ in the positive x-direction and that there is no attenuation.

As explained in Chapter II, there is a velocity potential $\phi(r,\theta,z,t)$ which satisfies the wave equation (2.4),

$$\nabla^2\phi = \frac{1}{c_o^2}\frac{\partial^2\phi}{\partial t^2}\,, \tag{3.1}$$

where ∇^2 is again the Laplacian operator in cylindrical polar coordinates (r,θ,z).

The boundary conditions for $\phi(r,\theta,z,t)$ are as follows:

$$\frac{\partial\phi}{\partial z}(r,\theta,0,t) = 0\,, \tag{3.2}$$

$$\frac{\partial^2\phi}{\partial t^2} + g\frac{\partial\phi}{\partial z} = 0 \quad \text{at} \quad z = h \ , \tag{3.3}$$

$$\frac{\partial\phi}{\partial r}(R,\theta,z,t) = -\frac{i}{\omega} a e^{i\omega t}\cos\theta \ , \tag{3.4}$$

and

$$\frac{1}{r}\frac{\partial\phi}{\partial\theta}(r, \pm\frac{\pi}{2}, z, t) = \pm\frac{i}{\omega} a e^{i\omega t} \ . \tag{3.5}$$

Let $\phi(r,\theta,z,t) = \phi_1(r,\theta,z,t) + \phi_2(r,\theta,z,t) + \phi_3(r,\theta,z,t)$, where ϕ_1, ϕ_2, and ϕ_3 each satisfies the governing equation (3.1),

$$\nabla^2\phi_i = \frac{1}{c_o^2}\frac{\partial^2\phi_i}{\partial t^2} \qquad (i = 1,2,3) \ . \tag{3.6}$$

$\phi_1(r,\theta,z,t)$ satisfies the boundary conditions (3.2) to (3.4) and

$$\frac{1}{r}\frac{\partial\phi_1}{\partial\theta}(r, \pm\frac{\pi}{2}, z, t) = 0 \ . \tag{3.7}$$

$\phi_2(r,\theta,z,t)$ and $\phi_3(r,\theta,z,t)$ each satisfies (3.2), (3.3) and also

$$\frac{1}{r}\frac{\partial\phi_2}{\partial\theta}(r, \pm\frac{\pi}{2}, z, t) = \pm\frac{i}{\omega} a e^{i\omega t} \ , \tag{3.8}$$

$$\frac{1}{r}\frac{\partial\phi_3}{\partial\theta}(r, \pm\frac{\pi}{2}, z, t) = 0 \ , \tag{3.9}$$

and

$$\frac{\partial\phi_3}{\partial r}(R,\theta,z,t) = -\frac{\partial\phi_2}{\partial r}(R,\theta,z,t) \ . \tag{3.10}$$

3.2 Velocity Potential and Pressure Distribution

The solutions of eq. (3.6) subject to the boundary conditions (3.2) - (3.5) and (3.7) - (3.10) are obtained by the method of separation of variables (see Appendix B) as

$$\phi_1(r,\theta,z,t) = \sum_{n=0}^{\infty} \left\{ \frac{4ia(-1)^n \varepsilon_n \cos(2n\theta) e^{i\omega t}}{\pi \omega h (4n^2 - 1)} \right.$$

$$\times \left[\frac{P_o J_{2n}(\mu_o r) \cosh \lambda_o z}{\lambda_o \mu_o (1 + CP_o^2) J'_{2n}(\mu_o R)} \right.$$

$$+ \sum_{m=1}^{M} \frac{P_m J_{2n}(\mu_m r) \cos \lambda_m z}{\lambda_m \mu_m (1 - CP_m^2) J'_{2n}(\mu_m R)}$$

$$\left. \left. + \sum_{m=M+1}^{\infty} \frac{P_m I_{2n}(\beta_m r) \cos \lambda_m z}{\lambda_m \beta_m (1 - CP_m^2) I'_{2n}(\beta_m R)} \right] \right\} , \qquad (3.11)$$

$$\phi_2(r,\theta,z,t) = -\frac{2a}{\omega h} e^{i\omega t} \left\{ \frac{P_o e^{i\mu_o r \cos\theta} \cosh \lambda_o z}{\lambda_o \mu_o (1 + CP_o^2)} \right.$$

$$+ \sum_{m=1}^{M} \frac{P_m e^{i\mu_m r \cos\theta} \cos \lambda_m z}{\lambda_m \mu_m (1 - CP_m^2)}$$

$$\left. - \sum_{m=M+1}^{\infty} \frac{i P_m e^{-\beta_m r \cos\theta} \cos \lambda_m z}{\lambda_m \beta_m (1 - CP_m^2)} \right\} , \qquad (3.12)$$

and

$$\phi_3(r,\theta,z,t) = \sum_{n=0}^{\infty} \left\{ \frac{2ia\ \ell_n \cos(2n\theta)}{\pi \omega h}\ e^{i\omega t} \left[\frac{P_o F_{on} J_{2n}(\mu_o r) \cosh \lambda_o z}{\lambda_o \mu_o (1 + CP_o^2) J'_{2n}(\mu_o R)} \right.\right.$$

$$\left.\left. + \sum_{m=1}^{\infty} \frac{P_m F_{mn} J_{2n}(\mu_m r) \cos \lambda_m z}{\lambda_m \mu_m (1 - CP_m^2)\ J'_{2n}(\mu_m R)} \right] \right\} , \qquad (3.13)$$

where

$$\ell_o = 1, \quad \ell_n = 2 \quad \text{for} \quad n \neq 0 , \qquad (3.14)$$

$$F_{mn} = 2 \int_o^{\pi/2} \cos\theta \cos(2n\theta)\ e^{i\mu_m R \cos\theta}\ d\theta \begin{pmatrix} m = 0,1,2\ldots \\ n = 0,1,2\ldots \end{pmatrix} . \qquad (3.15)$$

All the other parameters λ_o, λ_m, μ_o, μ_m, β_m, P_o and P_m have been defined in equations (2.14) - (2.20).

Let

$$F_{mn} = A_{mn} + iB_{mn} \quad \begin{pmatrix} m = 0,1,2\ldots \\ n = 0,1,2\ldots \end{pmatrix} , \qquad (3.16)$$

where A_{mn} and B_{mn} are real for real μ_m's. From equation (3.15) we obtain

$$A_{mn} = \frac{\pi}{2} (-1)^{n+1} \left[E_{2n-1}(\mu_m R) - E_{2n+1}(\mu_m R) \right]$$

$$= \pi(-1)^{n+1} E'_{2n}(\mu_m R) , \qquad (3.17)$$

where E_ν is Weber's function given by

$$E_\nu(x) = \frac{1}{\pi}\int_0^\pi \sin(\nu\theta - x\sin\theta)d\theta \ . \tag{3.18}$$

The prime denotes differentiation with respect to the argument. Also,

$$B_{mn} = \pi(-1)^{n+1} J'_{2n}(\mu_m R) \ . \tag{3.19}$$

When $\mu_m = i\beta_m$,

$$B_{mn} = i\pi I'_{2n}(\beta_m R) \tag{3.20}$$

and A_{mn} remains real. Hence, the integral F_{mn} is real when the argument $\mu_m R$ is purely imaginary. This is evident from Eq. (3.15).

The hydrodynamic pressure on the upstream face of the dam can be obtained as the real part of $-\rho_o \frac{\partial\phi}{\partial t}\Big|_{\theta = \pm\frac{\pi}{2}}$. Therefore,

$$P = \left\{ \sum_{n=0}^{\infty} \left\{ \frac{4\rho_o a\, \ell_n\, P_o J_{2n}(\mu_o r)\cosh\lambda_o z}{\pi h \mu_o \lambda_o (1 + CP_o^2) J'_{2n}(\mu_o R)} \left[\frac{1}{4n^2 - 1} - \frac{\pi E'_{2n}(\mu_o R)}{2} \right] \right. \right.$$

$$+ \sum_{m=1}^{M} \frac{4\rho_o a\, \ell_n\, P_m J_{2n}(\mu_m r)\cos\lambda_m z}{\pi h \mu_m \lambda_m (1 - CP_m^2) J'_{2n}(\mu_m R)} \left[\frac{1}{4n^2 - 1} - \frac{\pi E'_{2n}(\mu_m R)}{2} \right]$$

$$\left. + \sum_{m=M+1}^{\infty} \frac{4\rho_o a\, \ell_n\, P_m I_{2n}(\beta_m r)\cos\lambda_m z}{\pi h \beta_m \lambda_m (1 - CP_m^2) I'_{2n}(\beta_m R)} \left[\frac{1}{4n^2 - 1} + \frac{(-1)^n F_{mn}}{2} \right] \right.$$

(equation cont'd)

$$+ \sum_{m=M+1}^{\infty} \frac{2\rho_o a\, P_m}{h\beta_m \lambda_m (1 - CP_m^2)} \cos \lambda_m z \Bigg\} \cos \omega t$$

$$+ \Bigg\{ \sum_{n=0}^{\infty} \Bigg[\frac{2\rho_o a\, \ell_n\, P_o J_{2n}(\mu_o r)}{h\mu_o \lambda_o (1 + CP_o^2)} \cosh \lambda_o z$$

$$+ \sum_{m=1}^{M} \frac{2\rho_o a\, \ell_n\, P_m\, J_{2n}(\mu_m r)}{h\mu_m \lambda_m (1 - CP_m^2)} \cos \lambda_m z \Bigg]$$

$$- \Bigg[\frac{2\rho_o a\, P_o}{h\mu_o \lambda_o (1 + CP_o^2)} \cosh \lambda_o z + \sum_{m=1}^{M} \frac{2\rho_o a\, P_m}{h\mu_m \lambda_m (1 - CP_m^2)} \cos \lambda_m z \Bigg] \Bigg\}$$

$$\times \sin \omega t \quad . \tag{3.21}$$

We shall define the dimensionless in-phase component of the pressure coefficient C_{pi} and the out-of-phase component C_{po} by

$$C_{pi} \cos\omega t + C_{po} \sin\omega t = C_p = \frac{P(r, \pm \frac{\pi}{2}, z, t)}{\rho_o\, ah} \quad . \tag{3.22}$$

We can also write this in the form

$$C_{pi} \cos\omega t + C_{po} \sin\omega t = C_{pl} \cos(\omega t - \alpha) \ , \tag{3.23}$$

where

$$C_{pl} = \sqrt{C_{pi}^2 + C_{po}^2} \quad \text{and} \quad \alpha = \tan^{-1}(C_{po}/C_{pi}) \ . \tag{3.24}$$

Thus,

$$C_{pi} = \sum_{n=0}^{\infty} \left\{ \frac{4\ \ell_n\ P_o J_{2n}(\mu_o^* r^*)\cosh(\lambda_o^* z^*)}{\pi \mu_o^* \lambda_o^* (1 + CP_o^2) J'_{2n}(\mu_o^* R^*)} \right.$$

$$\times \left[\frac{1}{4n^2 - 1} - \frac{\pi E'_{2n}(\mu_o^* R^*)}{2} \right]$$

$$+ \sum_{m=1}^{M} \frac{4\ \ell_n\ P_m J_{2n}(\mu_m^* r^*)\cos(\lambda_m^* z^*)}{\pi \mu_m^* \lambda_m^* (1 - CP_m^2) J'_{2n}(\mu_m^* R^*)}$$

$$\times \left[\frac{1}{4n^2 - 1} - \frac{\pi E'_{2n}(\mu_m^* R^*)}{2} \right]$$

$$+ \sum_{m=M+1}^{\infty} \frac{4\ \ell_n\ P_m I_{2n}(\beta_m^* r^*)\cos(\lambda_m^* z^*)}{\pi \beta_m^* \lambda_m^* (1 - CP_m^2) I'_{2n}(\beta_m^* R^*)} \times \left[\frac{1}{4n^2 - 1} \right.$$

$$\left. \left. + \frac{(-1)^n F_{mn}}{2} \right] \right\} + \sum_{m=M+1}^{\infty} \frac{2\ P_m}{\beta_m^* \lambda_m^* (1 - CP_m^2)} \cos(\lambda_m^* z^*) \qquad (3.25)$$

and

$$C_{Po} = -\left[\frac{2\ P_o}{\mu_o^* \lambda_o^* (1 + CP_o^2)} \cosh(\lambda_o^* z^*) \right.$$

$$\left. + \sum_{m=1}^{M} \frac{2\ P_m}{\mu_m^* \lambda_m^* (1 - CP_m^2)} \cos(\lambda_m^* z^*) \right]$$

(equation cont'd)

$$+ \sum_{n=0}^{\infty} \left[\frac{2\, \ell_n\, P_o J_{2n}(\mu_o^* r^*)}{\mu_o^* \lambda_o^* (1 + CP_o^2)} \cosh(\lambda_o^* z^*) \right.$$

$$\left. + \sum_{m=1}^{M} \frac{2\, \ell_n\, P_m J_{2n}(\mu_m^* r^*)}{\mu_m^*\, \lambda_m^* (1 - CP_m^2)} \cos(\lambda_m^* z^*) \right] , \qquad (3.26)$$

where the dimensionless parameters λ_o^*, λ_m^*, μ_o^*, μ_m^*, β_m^*, R* and z* have been defined in eqs. (2.26) and

$$r^* = r/h \ . \qquad (3.27)$$

3.3 Hydrodynamic Force and Moment Coefficients

We can evaluate the dimensionless force coefficient from

$$C_F = \frac{1}{h} \int_o^h C_p dz$$

$$= C_{Fi} \cos\omega t + C_{Fo} \sin\omega t \ , \qquad (3.28)$$

where C_{Fi} is the in-phase component and C_{Fo} is the out-of-phase component of the force coefficient. We can also write C_F in the form of

$$C_F = C_{F1} \cos(\omega t - \beta) \ , \qquad (3.29)$$

where

$$C_{F1} = \sqrt{C_{Fi}^2 + C_{Fo}^2} \qquad \text{and} \qquad \beta = \tan^{-1}(C_{Fo}/C_{Fi}) \ . \qquad (3.30)$$

substituting (3.22), (3.25) and (3.26) into (3.28), we obtain

$$C_{Fi} = \sum_{n=0}^{\infty} \Bigg\{ \frac{4\,\ell_n\, P_o^2 J_{2n}(\mu_o^* r^*)}{\pi \mu_o^* \lambda_o^{*2} (1 + CP_o^2) J'_{2n}(\mu_o^* R^*)} \times \left[\frac{1}{4n^2 - 1} - \frac{\pi E'_{2n}(\mu_o^* R^*)}{2} \right]$$

$$+ \sum_{m=1}^{M} \frac{4\,\ell_n\, P_m^2 J_{2n}(\mu_m^* r^*)}{\pi \mu_m^* \lambda_m^{*2} (1 - CP_m^2) J'_{2n}(\mu_m^* R^*)} \times \left[\frac{1}{4n^2 - 1} - \frac{\pi E'_{2n}(\mu_m^* R^*)}{2} \right]$$

$$+ \sum_{m=M+1}^{\infty} \frac{4\,\ell_n\, P_m^2 I_{2n}(\beta_m^* r^*)}{\pi \beta_m^* \lambda_m^{*2} (1 - CP_m^2) I'_{2n}(\beta_m^* R^*)} \times \left[\frac{1}{4n^2 - 1} - \frac{(-1)^n F_{mn}}{2} \right] \Bigg\}$$

$$+ \sum_{m=M+1}^{\infty} \frac{2\, P_m^2}{\beta_m^* \lambda_m^{*2} (1 - CP_m^2)} \qquad (3.31)$$

and

$$C_{Fo} = -\left[\frac{2\,P_o^2}{\mu_o^*\lambda_o^{*2}(1 + CP_o^2)} + \sum_{m=1}^{M} \frac{2\,P_m^2}{\mu_m^*\lambda_m^{*2}(1 - CP_m^2)}\right]$$

$$+ \sum_{n=0}^{\infty}\left[\frac{2\,\ell_n\,P_o^2}{\mu_o^*\lambda_o^{*2}(1 + CP_o^2)}\,J_{2n}(\mu_o^* r^*)\right.$$

$$\left. + \sum_{m=1}^{M} \frac{2\,\ell_n\,P_m^2}{\mu_m^*\lambda_m^{*2}(1 - CP_m^2)}\,J_{2n}(\mu_m^* r^*)\right] . \qquad (3.32)$$

The dimensionless moment coefficient can similarly be evaluated from

$$C_M = \frac{1}{h^2}\int_o^h z\,C_p\,dz$$

$$= C_{Mi}\cos\omega t + C_{Mo}\sin\omega t , \qquad (3.33)$$

where C_{Mi} is the in-phase component and C_{Mo} is the out-of-phase component of the moment coefficient. We can also write C_M in the form

$$C_M = C_{Ml}\cos(\omega t - \gamma) , \qquad (3.34)$$

where

$$C_{Ml} = \sqrt{C_{Mi}^2 + C_{Mo}^2} \quad \text{and} \quad \gamma = \tan^{-1}(C_{Mo}/C_{Mi}) . \qquad (3.35)$$

Thus,

$$C_{Mi} = \sum_{n=0}^{\infty} \left\{ \frac{4\,\ell_n\,P_o\,J_{2n}(\mu_o^* r^*)G_o}{\pi\mu_o^*\lambda_o^{*3}(1 + CP_o^2)J'_{2n}(\mu_o^* R^*)} \right.$$

$$\times \left[\frac{1}{4n^2 - 1} - \frac{\pi E'_{2n}(\mu_o^* R^*)}{2} \right]$$

$$+ \sum_{m=1}^{M} \frac{4\ell_n\,P_m\,J_{2n}(\mu_m^* r^*)G_m}{\pi\mu_m^*\lambda_m^{*3}(1 - CP_m^2)J'_{2n}(\mu_m^* R^*)}$$

$$\times \left[\frac{1}{4n^2 - 1} - \frac{\pi E'_{2n}(\mu_m^* R^*)}{2} \right]$$

$$+ \sum_{m=M+1}^{\infty} \frac{4\,\ell_n\,P_m\,I_{2n}(\beta_m^* r^*)G_m}{\pi\beta_m^*\lambda_m^{*3}(1 - CP_m^2)I'_{2n}(\beta_m^* R^*)}$$

$$\left. \times \left[\frac{1}{4n^2 - 1} - \frac{(-1)^n F_{mn}}{2} \right] \right\} + \sum_{m=M+1}^{\infty} \frac{2\,P_m\,G_m}{\beta_m^*\lambda_m^{*3}(1 - CP_m^2)} \qquad (3.36)$$

and

$$C_{Mo} = -\left[\frac{2P_o\,G_o}{\mu_o^*\lambda_o^{*3}(1 + CP_o^2)} + \sum_{m=1}^{M} \frac{2P_m\,G_m}{\mu_m^*\lambda_m^{*3}(1 - CP_m^2)} \right]$$

$$+ \sum_{n=0}^{\infty} \left[\frac{2\,\ell_n\,P_o\,G_o}{\mu_o^*\lambda_o^{*3}(1 + CP_o^2)} J_{2n}(\mu_o^* r^*) \right.$$

$$\left. + \sum_{m=1}^{M} \frac{2\,\ell_n\,P_m\,G_m}{\mu_m^*\lambda_m^{*3}(1 - CP_m^2)} J_{2n}(\mu_m^* r^*) \right] , \qquad (3.37)$$

where

$$G_o = \lambda_o * P_o - Q_o + 1 \tag{3.38}$$

and

$$G_m = \lambda_m * P_m + Q_m - 1 \qquad (m = 1, 2, 3...) \; . \tag{3.39}$$

IV. DISCUSSION OF RESULTS

4.1 Circular Reservoir

The dimensionless pressure, force and moment coefficients are given by eqs. (2.25), (2.30), and (2.32), respectively. The local pressure coefficient C_p is dependent on the dimensionless parameters R*, z*, C and B. The force and moment coefficients, however, are independent of z* but depend on all the other parameters.

The period of the ground acceleration, T, during a typical earthquake may range from 0.1 sec to 10 seconds. If the reservoir height h is assumed to be 300 ft, then the maximum value of B is approximately 4 and that of C is 0.27. Since C is inversely proportional to h and B is directly proportional to h, the value of B increases and that of C decreases for a deeper reservoir. The maximum value of z* is 1; however, R* has no maximum.

The pressure distribution at the dam surface is shown in Fig. 5 for an incompressible fluid with no surface wave (B = 0, C = 0), for varying values of R*. It can be seen that the maximum value is attained at the bottom of the reservoir (z* = 0). Also, since surface waves are absent, the pressure at the surface is zero. The pressure, at any given height, increases with an increase in R*, until it reaches a maximum for a certain value of R*. Then, with further

increase in R*, the pressure reduces and attains a finite value as $R^* \to \infty$. The pressure coefficient at the bottom as $R^* \to \infty$ is 0.742. This is exactly the value given by Westergaard (1933), Chwang (1978) and Huang (1980) for an infinitely long reservoir with no surface waves. The corresponding force and moment coefficients are 0.543 and 0.218 respectively, which are precisely the values obtained by Huang (1980).

The behavior of the pressure distribution with increase in R* can be explained. Initially, the pressure increases as the amount of fluid in the reservoir increases, as long as the total mass in the reservoir is less than the "added" mass". It keeps increasing until the total mass exceeds the "added mass". There is another factor affecting the pressure at the dam surface. This is the curvature of the side walls near the dam. When the reservoir is small, there is a component of the hydrodynamic pressure at the dam surface, due to the side walls. However, when the reservoir is large enough, this effect is negligible. Hence, the pressure reduces and stabilizes as $R^* \to \infty$.

In Fig. 6, the value of C_p at the bottom of the reservoir for increasing values of R* is shown. It can be noted that C_p, as $R^* \to \infty$, is 0.742 as already mentioned. The values of R* for which C_p reaches a maximum at the bottom of the reservoir have been plotted (see Fig. 7) for increasing values of B. It is noted that, for increasing B, the maximum C_p occurs at increasing values of R*.

The variation of the pressure coefficient C_p with the compressibility parameter B can be seen in Fig. 8 ($R^* = 5$, $C = 0$). The pressure

increases with B until it reaches resonant values of the reservoir. The corresponding force and moment coefficients have been plotted in Fig. 9. Figure 10 shows the same variation of C_p as in Fig. 8, but for $C = 0.05$ and $R^* = 5$. The corresponding force and moment coefficients (see Fig. 11) are seen to reach resonant values.

Investigating the nature of the roots of eq. (2.14) from Fig. 12, we notice that it yields only one root λ_0^*. From Fig. 13, we see that eq. (2.15) yields infinitely many roots λ_m^* ($m = 1,2,3...$). These roots λ_m^* lie between $(2m-1)\pi/2$ and $m\pi$ ($m = 1,2,3...$). When $C = 0$, the roots are

$$\lambda_m^* = \frac{(2m-1)\pi}{2} \quad (m = 1,2,3...) \; . \tag{4.1}$$

Hence, the series for m from 1 to M in eq. (2.25) exists only when $B > \lambda_1^*$. When $B > \lambda_m^*$, the term $J_0(\mu_m^* R^*) - J_2(\mu_m^* R^*)$ [$= 2J_1'(\mu_m^* R^*)$], will give rise to some resonant frequencies. Let us consider the case when $C = 0$ and $R^* = 5$. Resonance occurs for $B = 1.6134, 1.8985, \ldots,$. When $C \neq 0$, resonance will occur at slightly higher values of B. If R^* is very large, then resonance occurs at $B \doteq \lambda_m^*$ ($m = 1,2,3...$). When $C \neq 0$, resonance also occurs when $J_1'(\mu_0^* R^*)$ vanishes.

The variation of C_p with the wave-effect parameter C is shown in Fig. 14. It should be noted that the pressure at the water surface is no longer zero when surface waves are present. In fact, the surface waves can play an important role as seen in the curve for $C = 0.35$. Also, the pressure distribution becomes oscillatory for large values of C.

4.2 Semi-circular Reservoir

The pressure, force and moment coefficients are given by eqs. (3.25), (3.26), (3.31), (3.32), (3.36) and (3.37). Also, there is an out-of-phase component for each of the three coefficients. The pressure coefficient C_{p1} is dependent on the dimensionless parameters R*, r*, z*, C and B. The force and moment coefficients, C_{F1} and C_{M1} respectively, however, are independent of z* but depend on all the other parameters.

The in-phase component of the pressure coefficient C_{pi} at the dam surface is shown in Fig. 15 for a reservoir of size R* = 1.0, at varying locations r/R. The fluid is considered to be incompressible with no surface waves (B = 0, C = 0). The maximum value for any fixed location r/R is attained at the bottom of the reservoir (z* = 0). Also, the maximum C_{pi}, at any given height, occurs at the central plane of the dam (r/R = 0). For larger values of R*, C_{pi} decreases slightly as r/R increases from zero to one at any fixed height. The out-of-phase component C_{p0} is zero for the values considered. Hence, Fig. 15 is also a graph of the total pressure coefficient C_{p1}.

For different values of B and C, the out-of-phase coefficient C_{p0}, was found to be negligible for small values of B and C. Its maximum was found to occur at the surface of the reservoir (z* = 1) and goes to zero at the bottom (z* = 0). Hence, the contribution of the out-of-phase component C_{F0} to the total force coefficient C_{F1} is even smaller. For large values of R*, the out-of-phase pressure

coefficient was found to be negligible for small r/R but oscillates about a small finite value as $r/R \to 1$ and $R^* \to \infty$.

At the central plane of the dam, the out-of-phase components of the pressure, force and moment coefficients are identically zero. This fact can be observed from eqs. (3.26), (3.32) and (3.37) respectively. Thus, at the central plane of the dam ($r^* = 0$), the in-phase component of the pressure coefficient C_{pi} is the total coefficient C_{pl} with $\alpha = 0$. Also, the in-phase components of the force and moment coefficients, C_{Fi} and C_{Mi} respectively, are the total coefficients C_{Fl} and C_{Ml} respectively with $\beta = \gamma = 0$. All subsequent figures have been drawn at the central plane of the dam.

The pressure distribution for varying values of R*, at the central plane of the dam, is shown in Fig. 16. The fluid is considered to be incompressible with no surface waves ($B = 0$, $C = 0$). The pressure, at any given height, increases with R*. It attains a maximum value as $R^* \to \infty$. The maximum value of the pressure coefficient C_{pi} at the bottom of the reservoir is 0.742. The corresponding force and moment coefficients have been plotted in Fig. 17. The maximum values of the force and moment coefficients are 0.543 and 0.218 respectively.

The pressure distribution for a compressible fluid in the presence of surface waves ($B = 0.4$, $C = 0.05$, $r^* = 0$), for varying values of R*, is shown in Fig. 18. Since surface waves are present, the pressure at the undisturbed surface is ($z^* = 1$) is not zero. Also, the pressure at any given height is less than that for an incompressible

fluid. This is because the surface waves radiate some of the energy. On the other hand, the same trend as in Fig. 17 can be noticed in Fig. 18.

The variation of the pressure coefficient C_{pi} with the compressibility parameter B is shown in Fig. 19 ($R^* = 5$, $r^* = 0$, $C = 0.05$). The pressure increases with B till it reaches resonant values. This can be clearly seen in Fig. 20 which shows the corresponding force and moment coefficients. With further increase in B, resonant frequencies are encountered. The trend followed with increasing B is the same as in Fig. 11 except that resonance occurs at different values of B.

The roots λ_m^* ($m = 0,1,2,3,\ldots$) in eqs. (3.25), (3.26), (3.31), (3.32), (3.36) and (3.37), are the same as those described in the previous section and can be obtained as shown in Figs. 12 and 13. When $B > \lambda_m^*$, the term $J'_{2n}(\mu_m^* R^*)$ in eq. (3.25) will give rise to resonance. If we consider the particular case shown in Fig. 19 ($R^* = 5$, $C = 0.05$, $r^* = 0$), we see that resonance occurs for $J'_0(\mu_m^* R^*) = 0$ or $B = 1.8421, 2.0075, \ldots$, also for $J'_2(\mu_m^* R^*) = 0$ or $B = 1.7994, 1.9920, \ldots$, etc. Resonance also occurs when $J'_{2n}(\mu_0^* R^*)$ vanishes.

The variation of C_{pi} with the wave-effect parameter C is shown in Fig. 21 ($B = 0.4$, $R^* = 5$, $r^* = 0$). The pressure at the undisturbed surface is no longer zero when $C \neq 0$. The wave-effect parameter C causes the pressure distribution to be oscillatory and can be important for large values of C.

4.3 Comparison of Results

It can be noticed from Figs. 5 and 16 that for an incompressible fluid with no surface waves (B = 0, C = 0), the pressure coefficient attains a value of 0.742 at the base of a dam for an infinite reservoir. The corresponding force and moment coefficients are 0.543 and 0.218 respectively. These values agree exactly with those obtained by Westergaard (1933), Chwang (1978) and Huang (1980). However, in the case of the circular reservoir, these are not the maximum values. This is due to the effect of the side walls, as already explained in Section 4.1. In the case of the semi-circular reservoir, this effect, at the central plane of the dam, is negligible. This is because the walls in the vicinity are straight. Due to this effect, some variation in pressure can be noticed for $R^* > 10$ in the case of the circular reservoir, which is not so for the semi-circular reservoir.

In the semi-circular reservoir, out-of-phase components of the pressure, force and moment coefficients are present. However, these are negligible for low values of C and B and vanish altogether at the central plane of the dam. In the circular case, there is no out-of-phase component since this is a symmetric case with no discontinuities in the boundary.

Resonance in the circular case occurs for $J_1'(\mu_m R^*) = 0$. For C = 0.05, $R^* = 5$, this corresponds to B = 1.7306, 1.9218, ..., . In the semi-circular case, however, resonance occurs for $J_0'(\mu_m R^*) = 0$, $J_2'(\mu_m R^*) = 0$, etc. For C = 0.05, $R^* = 5$, this corresponds to

values of B = 1.7994, 1.8421, 1.9920, 2.0075, ..., etc. As can be easily noticed, resonance occurs for slightly higher values of B. Moreover, in the semi-circular case, more resonant frequencies are existent. All in all, the results from the two cases considered are quite similar.

V. CONCLUSIONS AND RECOMMENDATIONS

The hydrodynamic effect of earthquakes on three-dimensional dam-reservoir systems has been studied analytically in this thesis. The effects of surface waves and compressibility of the fluid in the reservoir have also been included. In the case of the dam-reservoir system with no surface waves, it was found that the in-phase component of the hydrodynamic pressure increases with the depth of the reservoir and attains a maximum value at the bottom. In the presence of surface waves, for small C, these values were slightly reduced. However, for larger values of C, the pressure distribution was found to be oscillatory.

The hydrodynamic forces were found to be insensitive to R/h when R/h was greater than 10. Only small reservoirs (R/h < 10) were influenced considerably by R/h. These reservoir sizes, however, are unusual in practice.

Resonances were found to occur for values of B greater than λ_1^*, whose minimum value was found to be $\pi/2$. Taking the value of the velocity of sound in water to be 1440 m/sec, we find that for dam-reservoir systems having h/T greater than 360 m/sec, resonances can occur. Here T is the time period of the ground motion. Hence, we should have low dam designs whenever possible. However, for deeper dam designs we can expect resonance to occur. Theoretically, the

resonant values of the hydrodynamic forces are infinite. In actual practice, there is some viscous damping in the fluid. Hence, these values will not be as large as the theoretical values. Also, considering the interaction between the dam and the reservoir might yield finite values of forces at the natural frequencies.

In this thesis, the dam has been assumed to be rigid. This assumption is good provided the fundamental natural frequency of the dam is much higher than that of the reservoir. However, this frequency may be close to that of the reservoir. Hence, the interaction between the reservoir and the flexible dam should be studied.

The reservoirs considered were ones with regular boundaries. In actual practice, the reservoirs have irregular boundaries. Hence, the hydrodynamic forces due to a dam-reservoir system with irregular boundaries should be studied in the future.

APPENDIX A

DERIVATION OF EQUATION (2.13)

In cylindrical co-ordinates, eq. (2.4) may be written as

$$\frac{\partial^2\phi}{\partial r^2} + \frac{1}{r}\frac{\partial\phi}{\partial r} + \frac{1}{r^2}\frac{\partial^2\phi}{\partial\theta^2} + \frac{\partial^2\phi}{\partial z^2} = \frac{1}{c_o^2}\frac{\partial^2\phi}{\partial t^2} . \tag{A.1}$$

By the method of separation of variables, we can obtain a solution of (A.1) which satisfies the boundary conditions (2.5), (2.6), (2.9) and the form of (2.12),

$$\phi(r,\theta,z,t) = X(r)\cos\theta \begin{Bmatrix} \cos\lambda z \\ \cosh\lambda z \end{Bmatrix} e^{i\omega t} , \tag{A.2}$$

where $X(r)$ is given by the Bessel differential equation,

$$r^2X'' + rX' + \left[\left(\frac{\omega^2}{c_o^2} \mp \lambda^2\right) - 1\right] X = 0 \tag{A.3}$$

and the primes denote derivatives with respect to the argument. The $\mp$ signs are associated with $\cos\lambda z$ and $\cosh\lambda z$, respectively. Here $\lambda = \lambda_o$ (eq. (2.14)) with the + sign and $\lambda = \lambda_m$ (eq. (2.15)) with the - sign. The solutions of (A.3) which are finite at $r = 0$ are then $J_1(\mu_o r)$ and $J_1(\mu_m r)$ or $I_1(\beta_m r)$ according as $\frac{\omega^2}{c_o^2} - \lambda^2 \gtrless 0$, where μ_o, μ_m and β_m are defined in (2.18), (2.19) and (2.20), respectively.

Thus, we get ϕ of the form

$$\phi = \{A_o \cosh \lambda_o z\, J_1(\mu_o r) + \sum_{m=1}^{M} A_m \cos \lambda_m z\, J_1(\mu_m r) + \sum_{m=M+1}^{\infty} A_m \cos \lambda_m z\, I_1(\beta_m r)\}\cos\theta\, e^{i\omega t} \quad . \tag{A.4}$$

Substitution into eq. (2.12) yields

$$\frac{A_o\mu_o}{2} \cosh \lambda_o z\, [J_o(\mu_o R) - J_2(\mu_o R)] + \sum_{m=1}^{M} \frac{A_m\mu_m}{2} \cos \lambda_m z \times [J_o(\mu_m R) - J_2(\mu_m R)] + \sum_{m=M+1}^{\infty} \frac{A_m\beta_m}{2} \cos \lambda_m z \times [I_o(\beta_m R) + I_2(\beta_m R) = \frac{i}{\omega} a e^{i\omega t} \tag{A.5}$$

Now, we will prove the orthogonality of $\begin{Bmatrix} \cosh \lambda_o z \\ \cos \lambda_m z \end{Bmatrix}$ over the interval 0 to h.

$$\int_0^h \cos \lambda_m z \cos \lambda_p z\, dz = \frac{\sin(\lambda_m-\lambda_p)h}{2(\lambda_m-\lambda_p)} + \frac{\sin(\lambda_m+\lambda_p)h}{2(\lambda_m+\lambda_p)}$$

$$= \frac{(\lambda_m+\lambda_p)\sin(\lambda_m-\lambda_p)h + (\lambda_m-\lambda_p)\sin(\lambda_m+\lambda_p)h}{2(\lambda_m^2 - \lambda_p^2)}$$

$$= \frac{\lambda_m \sin \lambda_m h \cos \lambda_p h - \lambda_p \cos \lambda_m h \sin \lambda_p h}{\lambda_m^2 - \lambda_p^2}$$

Substituting for $\cos \lambda_p h$ and $\cos \lambda_m h$ from eq. (2.15), we obtain

$$\int_0^h \cos \lambda_m z \cos \lambda_p z \, dz$$

$$= \frac{-\lambda_m \sin\lambda_m h[C\lambda_m h \sin\lambda_p h] + \lambda_p[C\lambda_m h \sin\lambda_m h]\sin\lambda_p h}{\lambda_m^2 - \lambda_p^2}$$

$$= 0 \qquad \text{when} \quad m \neq P \ .$$

When $m = P$,

$$\int_0^h \cos^2 \lambda_m z \, dz = \frac{h}{2} + \frac{\sin 2\lambda_m h}{4\lambda_m}$$

$$= \frac{\lambda_m h + \sin \lambda_m h \cos \lambda_m h}{2 \lambda_m} \ .$$

By using eq. (2.15) to replace $\cos \lambda_m h$, we obtain

$$\int_0^h \cos^2 \lambda_m z \, d_z = \frac{\lambda_m h - C\lambda_m h \sin^2 \lambda_m h}{2\lambda_m}$$

$$= \frac{h}{2} (1 - CP_m^2),$$

where P_m is defined in eq. (2.17).

Now consider

$$\int_0^h \cosh \lambda_o z \cos \lambda_m z \, dz$$

$$= \frac{\lambda_o \sinh \lambda_o h \cos \lambda_m h + \lambda_m \cosh \lambda_o h \sin \lambda_m h}{\lambda_o^2 + \lambda_m^2} .$$

Substituting for $\cos \lambda_m h$ from eq. (2.15) and $\cosh \lambda_o h$ from eq. (2.14), we obtain

$$\int_0^h \cosh \lambda_o z \cos \lambda_m z \, dz$$

$$= \frac{-\lambda_o \sinh \lambda_o h[C\lambda_m h \sin \lambda_m h] + \lambda_m [C\lambda_o h \sinh \lambda_o h] \sin \lambda_m h}{\lambda_o^2 + \lambda_m^2}$$

$$= 0$$

Now consider

$$\int_0^h \cosh^2 \lambda_o z \, dz = \frac{h}{2} (1 + CP_o^2) ,$$

where P_o is given in eq. (2.16).

Using all the above orthogonality conditions, the solution to eq. (A.5) is obtained as eq. (2.13).

APPENDIX B

DERIVATION OF EQUATIONS (3.11), (3.12) and (3.13)

The velocity potential ϕ_1, which satisfies the governing differential equation (3.6) and the boundary conditions (3.2) to (3.4) and (3.7), can be obtained by the method of separation of variables in the form

$$\phi_1(r,\theta,z,t) = Y(r)\cos(2n\theta)\begin{Bmatrix}\cos \lambda z \\ \cosh \lambda z\end{Bmatrix} e^{i\omega t} . \tag{B.1}$$

The factor $\cos(2n\theta)$ is obtained by using (3.7) and symmetry about $\theta = 0$. The same procedure as in Appendix A can now be applied to obtain the final form of (3.11).

The velocity potential ϕ_2 satisfies the governing differential equation (A.1). The solution for ϕ_2, also found by separating variables, is of the form

$$\phi_2(r,\theta,z,t) = F(r,\theta)\begin{Bmatrix}\cosh \lambda z \\ \cos \lambda z\end{Bmatrix} e^{i\omega t}, \tag{B.2}$$

where $F(r,\theta)$ satisfies the Helmholtz equation

$$\frac{\partial^2 F}{\partial r^2} + \frac{1}{r}\frac{\partial F}{\partial r} + \frac{1}{r^2}\frac{\partial^2 F}{\partial \theta^2} + \mu^2 F = 0 \tag{B.3}$$

Solutions of eq. (B.3) are of the form $e^{i\mu r\cos\theta}$ and $e^{i\mu r\sin\theta}$. Then, by using eq. (3.5) and the same orthogonality properties as in Appendix A, we get the final form for ϕ_2 given in eq. (3.12).

Since $\frac{\partial\phi_2}{\partial r}$ at r = R is not zero, an additional velocity potential ϕ_3 has been added such that

$$\left.\frac{\partial\phi_3}{\partial r}\right|_{r=R} = -\left.\frac{\partial\phi_2}{\partial r}\right|_{r=R}$$

$$= -\frac{2a}{\omega h} e^{i\omega t}\left\{\frac{i\,P_o}{\lambda_o(1+CP_o^{\,2})} e^{i\mu_o R\cos\theta}\cosh\lambda_o z\right.$$

$$+\left[\sum_{m=1}^{M}\frac{i\,P_m}{\lambda_m(1-CP_m^{\,2})} e^{i\mu_m R\cos\theta}\right.$$

$$\left.\left.+\sum_{m=M+1}^{\infty}\frac{i\,P_m}{\lambda_m(1-CP_m^{\,2})} e^{-\beta_m R\cos\theta}\right]\cos\lambda_m z\right\}\cos\theta \quad . \quad (B.4)$$

By separating variables, we can show that ϕ_3 may be expressed in the form

$$\phi_3(r,\theta,z,t) = \sum_{n=0}^{\infty}\left\{C_{on}J_{2n}(\mu_o r)\cosh\lambda_o z\right.$$

$$+\left[\sum_{m=1}^{M} C_{mn}\,J_{2n}(\mu_m r)\right.$$

$$\left.\left.+\sum_{m=M+1}^{\infty} C_{mn}I_{2n}(\beta_m r)\right]\cos\lambda_m z\right\}\cos(2n\theta)e^{i\omega t} \quad (B.5)$$

Then, using the same orthogonality properties for cos λz and cosh λz as in Appendix A, as also the orthogonality of cos$(2n\theta)$ over the interval $-\frac{\pi}{2}$ to $\frac{\pi}{2}$, we can evaluate the constants C_{mn} and obtain the final form of eq. (3.13).

REFERENCES

Chopra, A. K., 1967, Hydrodynamic pressures on dams during earthquakes, J. Eng. Mech. Division, ASCE, 93, 205-223.

Chwang, A. T., 1978, Hydrodynamic pressures on sloping dams during earthquakes. Part 2: Exact theory, J. Fluid Mech., 87, 343-348.

Chwang, A. T., 1979, Hydrodynamic pressure on an accelerating dam and criteria for cavitation, J. Eng. Math., 13, 143-152.

Chwang, A. T. and Housner, G. W., 1978. Hydrodynamic pressures on sloping dams during earthquakes. Part 1: Momentum method, J. Fluid Mech., 87, 335-341.

Huang, T. H., 1980, Earthquake effects on rectangular dam-reservoir systems, M.S. thesis, The University of Iowa, Iowa City.

Kármán, T. von, 1933, Discussion of water pressures on dams during earthquakes, Trans. ASCE, 98, 434-436.

Kotsubo, S., 1959, Dynamic water pressures on dams due to irregular earthquakes, Memoirs Faculty of Engineering, Kyushu University, Fukuoka, Japan, 18, 119-129.

Werner, P. W. and Sundquist, K. J., 1949, On hydrodynamic earthquake effects, Trans. American Geophysical Union, 30, 636-657.

Westergaard, H. M., 1933, Water pressures on dams during earthquakes, Trans. ASCE, 98, 418-433.

Zangar, C. N., 1953, Hydrodynamic pressures on dams due to horizontal earthquakes, Proc. Soc. Exp. Stress Anal., 10, 93-102.

Zangar, C. N. and Haefeli, R. J., 1952, Electric analog indicates effect of horizontal earthquake shock on dams, Civil Eng. 22, 278-279.

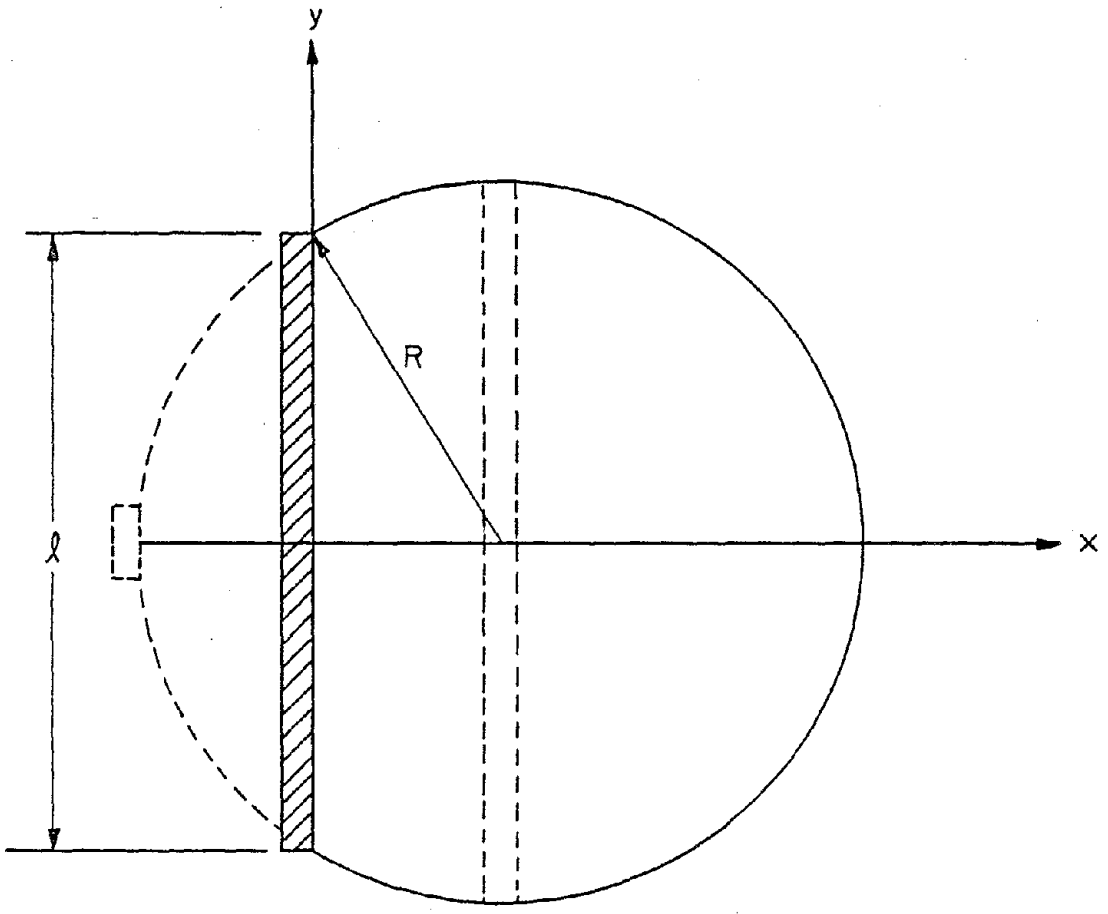

Figure 1. Schematic diagram of dam-reservoir systems with partly circular boundaries.

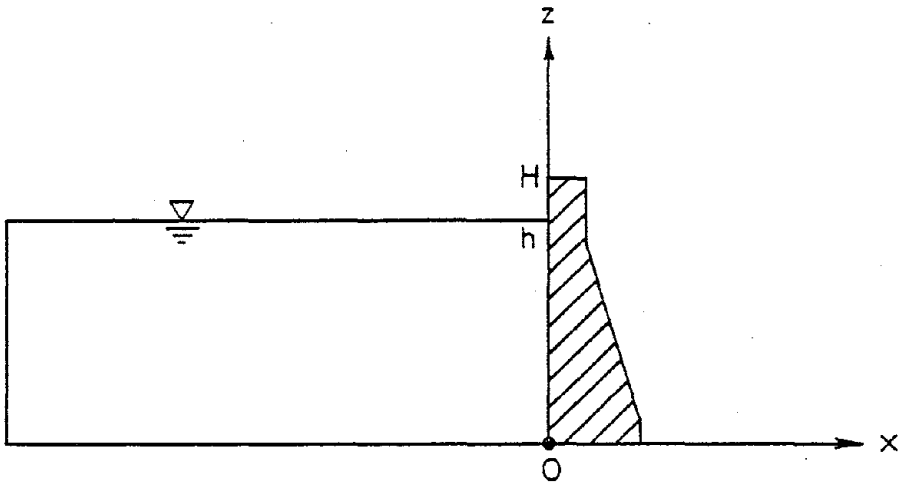

(a) Elevation

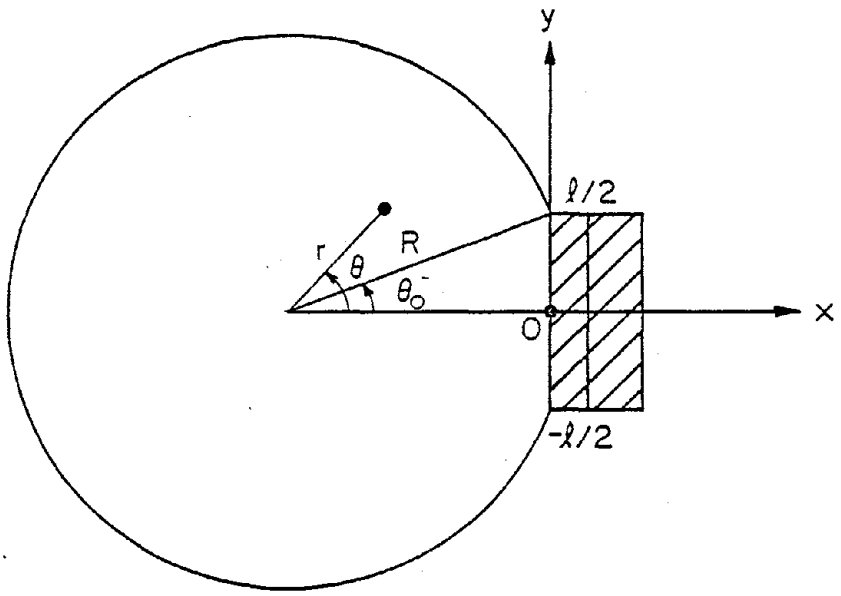

(b) Plan

Figure 2. Schematic diagram of a circular dam-reservoir system. (a) Elevation, (b) Plan.

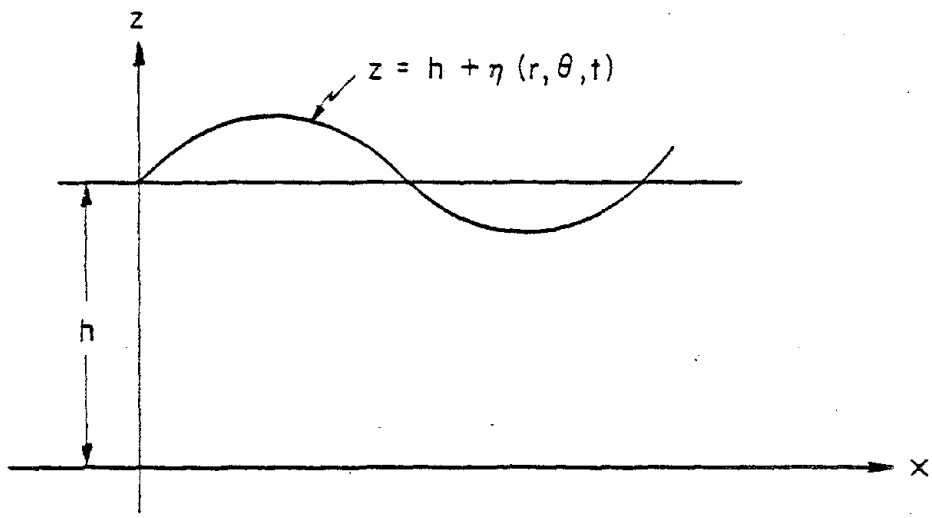

Figure 3. Schematic diagram of the free surface with surface waves.

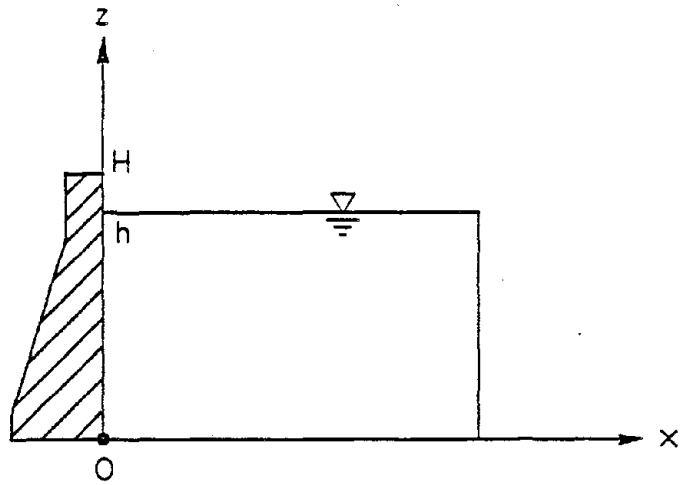

(a) Elevation

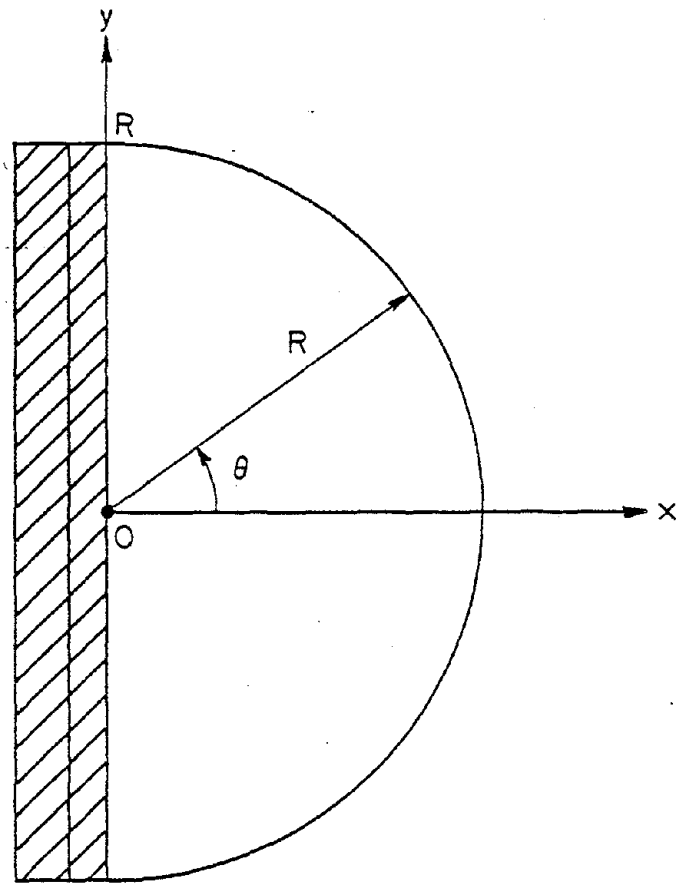

(b) Plan

Figure 4. Schematic diagram of a semi-circular dam-reservoir system. (a) Elevation, (b) Plan.

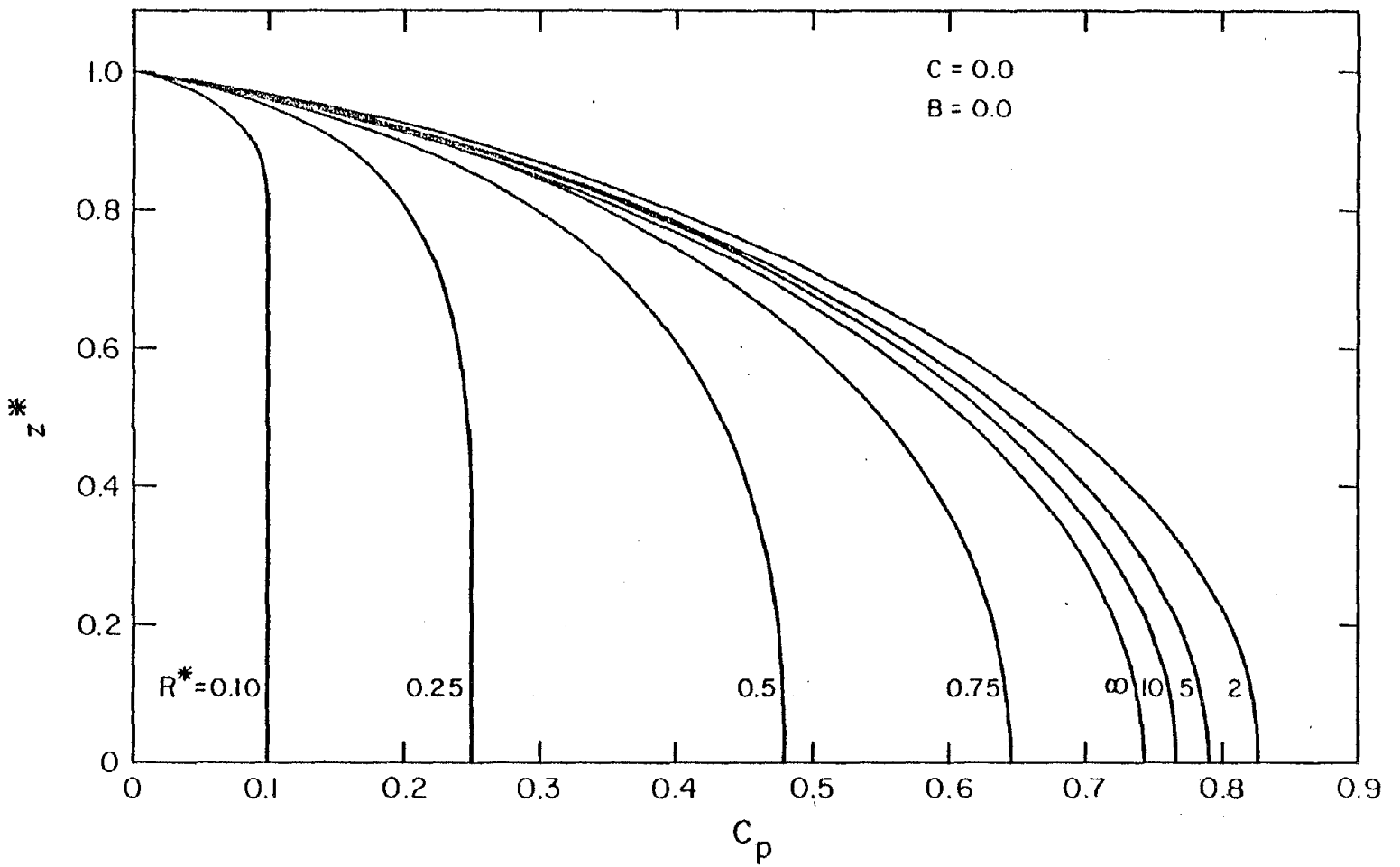

Figure 5. Variation of the pressure coefficient C_p with z*, for different values of R*. (Circular reservoir; C = 0.0, B = 0.0).

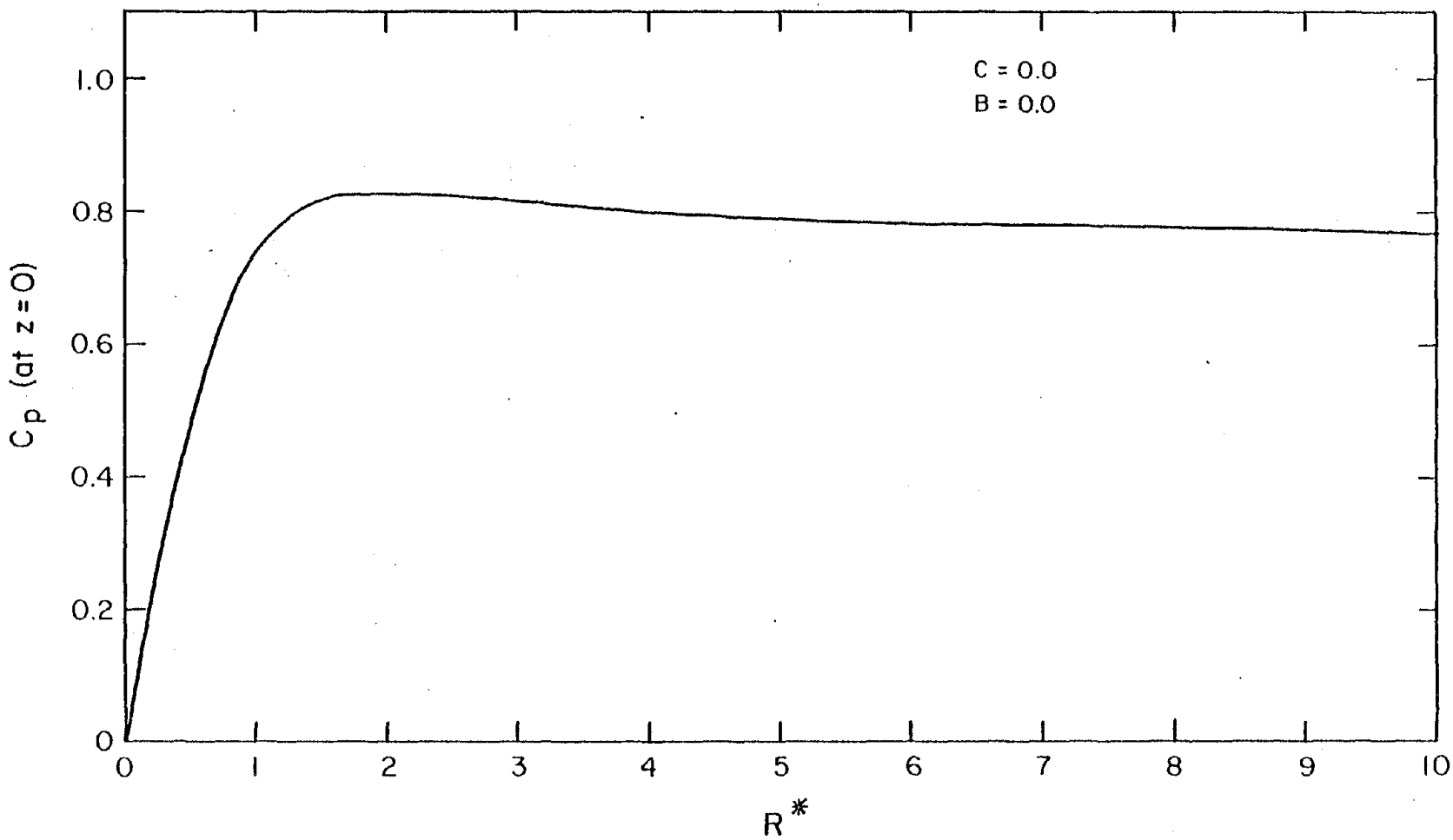

Figure 6. Variation of the pressure coefficient C_p at the bottom of the reservoir (z = 0), with R*. (Circular reservoir; C = 0.0, B = 0.0).

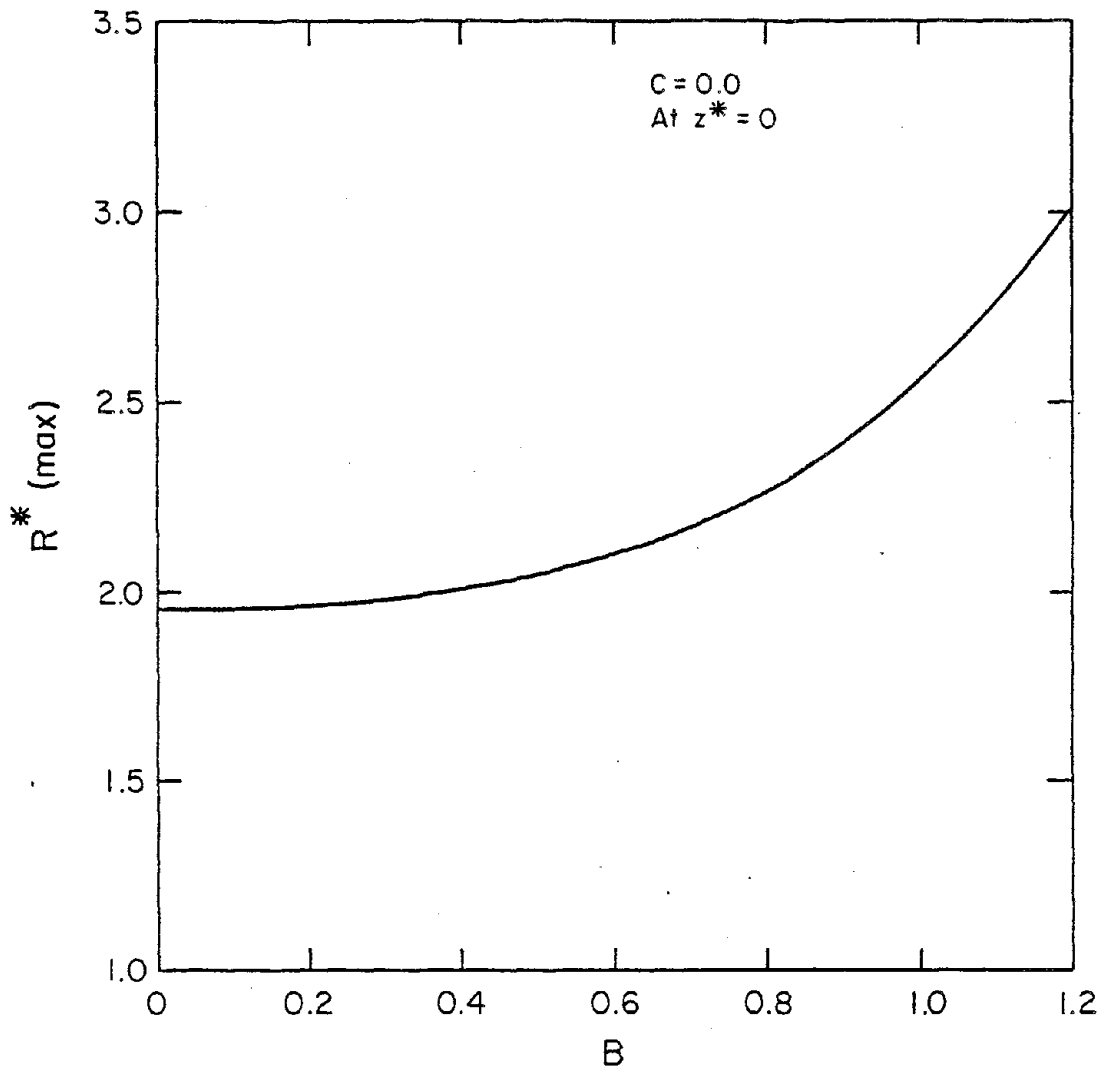

Figure 7. Variation of R* with the compressibility parameter B, for maximum value of the pressure coefficient C_p at z = 0. (Circular reservoir; C = 0.0).

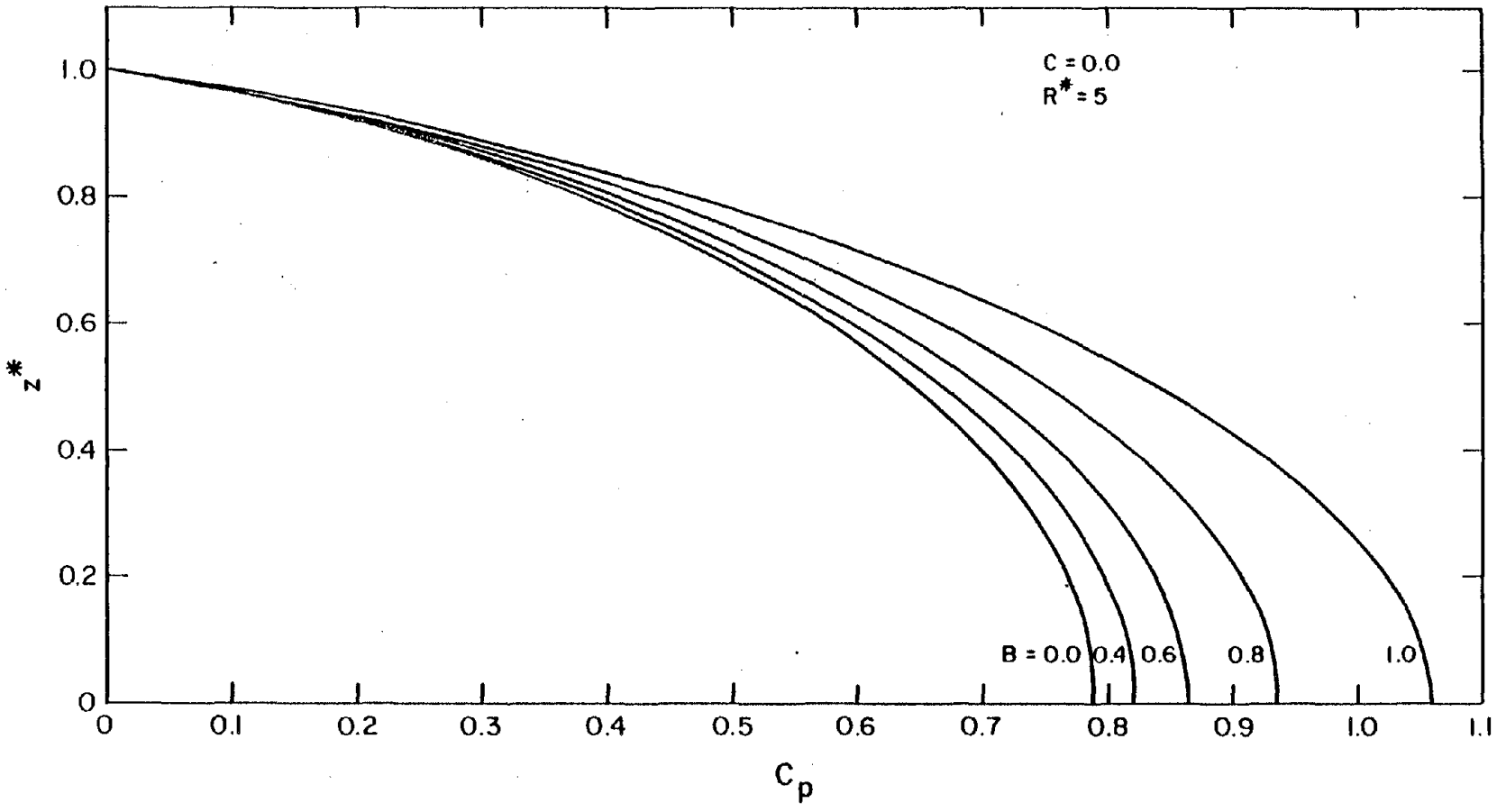

Figure 8. Variation of the pressure coefficient C_p with z*, for different values of the compressibility parameter B. (Circular reservoir; C = 0.0, R* = 5.0).

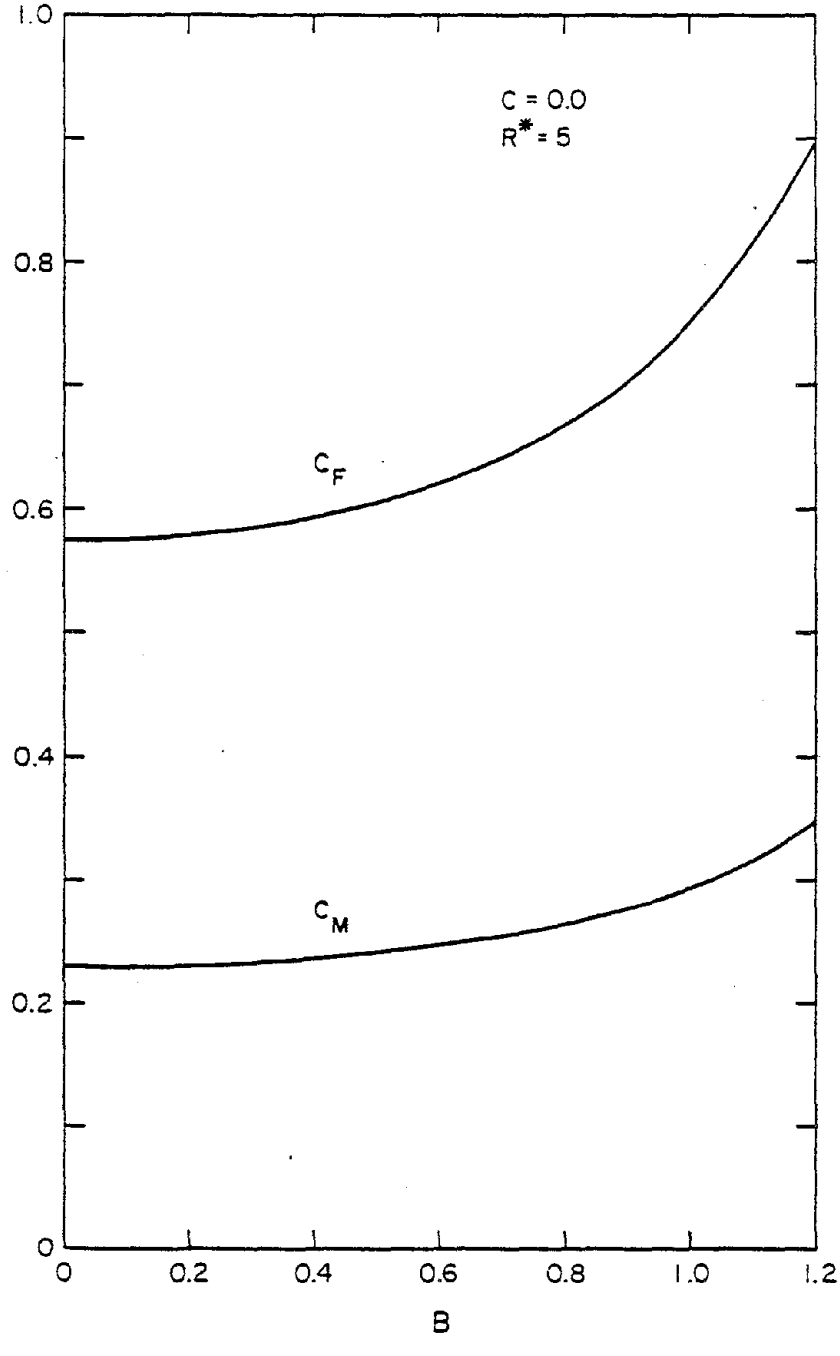

Figure 9. Variation of the force and moment coefficients, C_F and C_M respectively, with the compressibility parameter B. (Circular reservoir; C = 0.0, R* = 5.0).

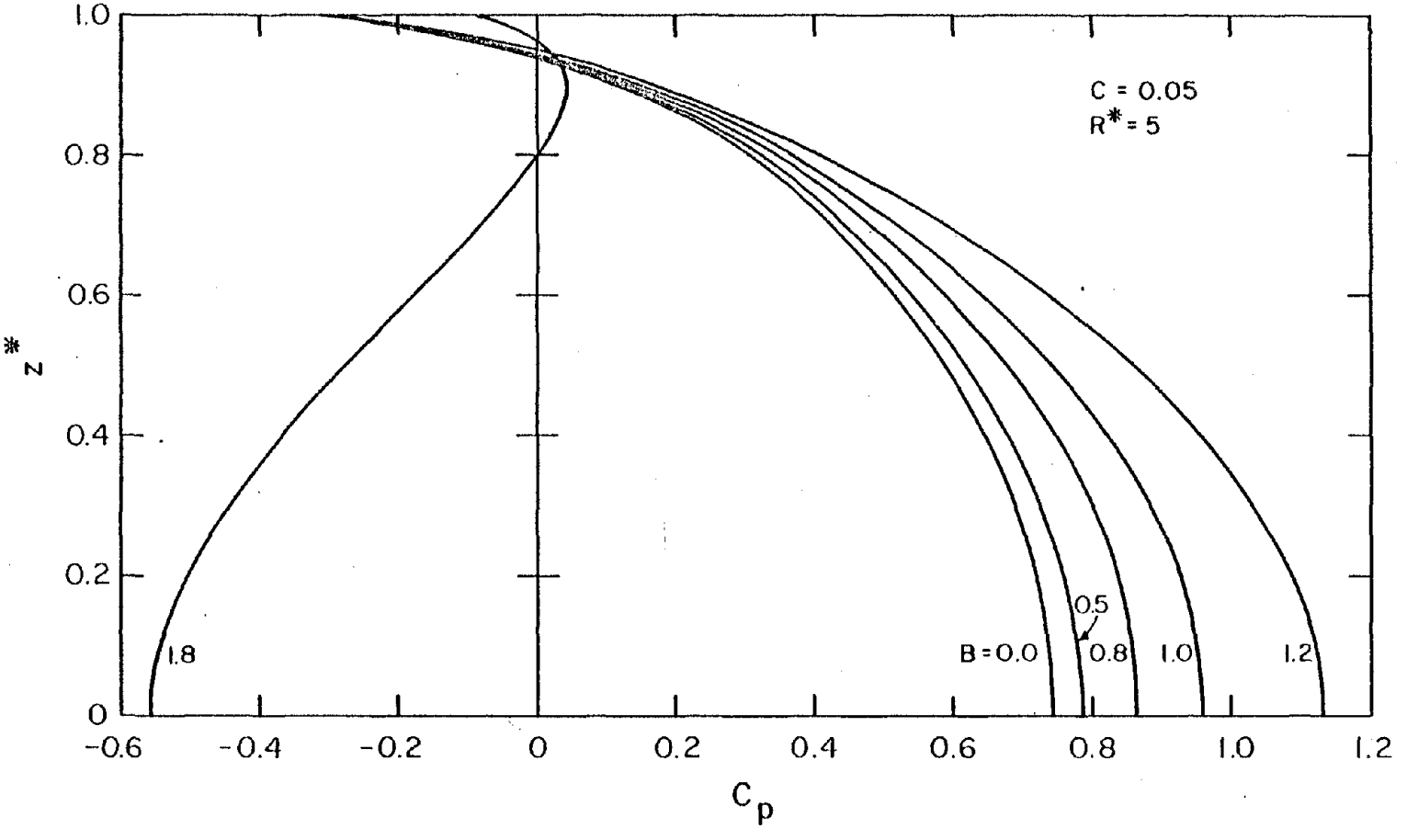

Figure 10. Variation of the pressure coefficient C_p with z*, for different values of the compressibility parameter B. (Circular reservoir; C = 0.05, R* = 5.0).

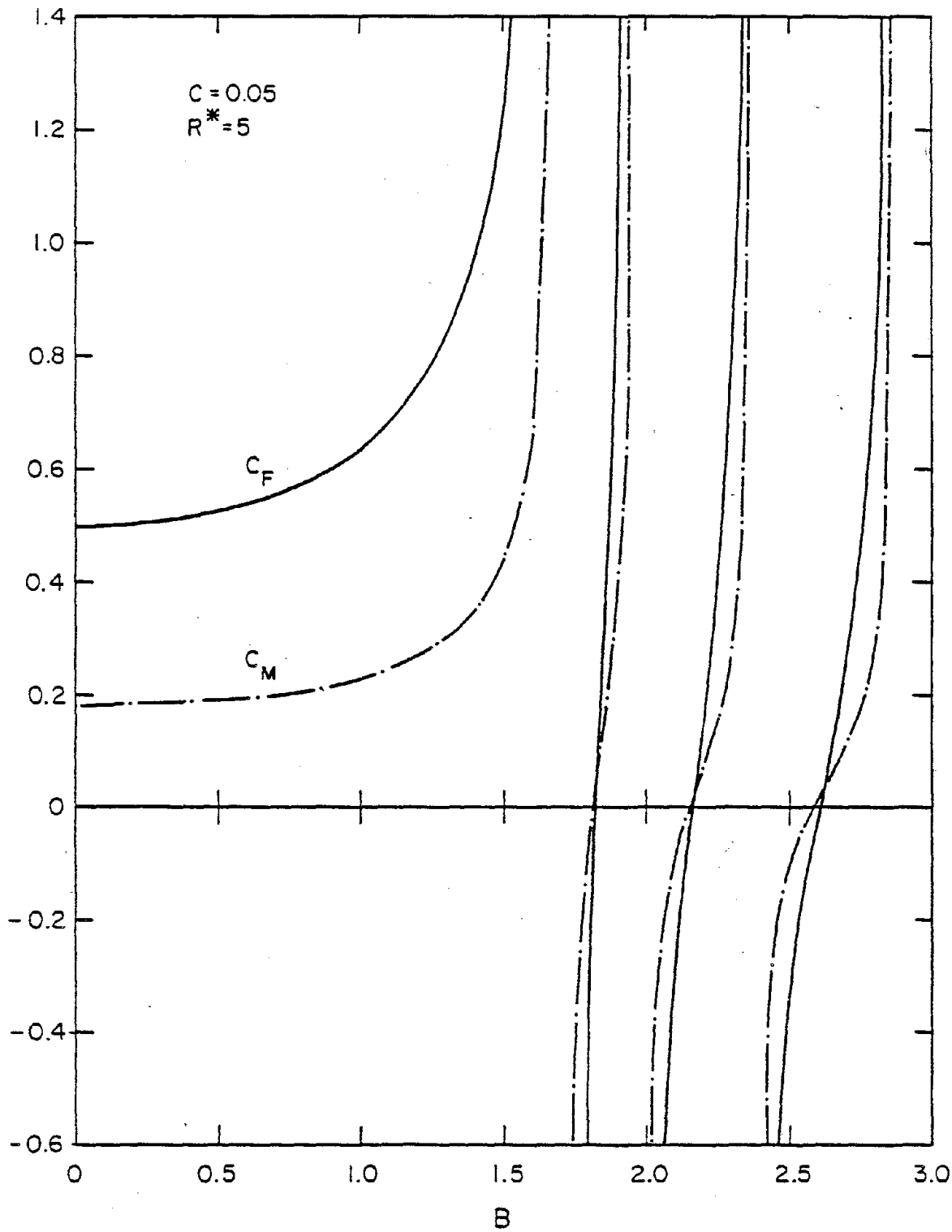

Figure 11. Variation of the force and moment coefficients, C_F and C_M respectively, with the compressibility parameter B. (Circular reservoir; C = 0.05, R* = 5.0).

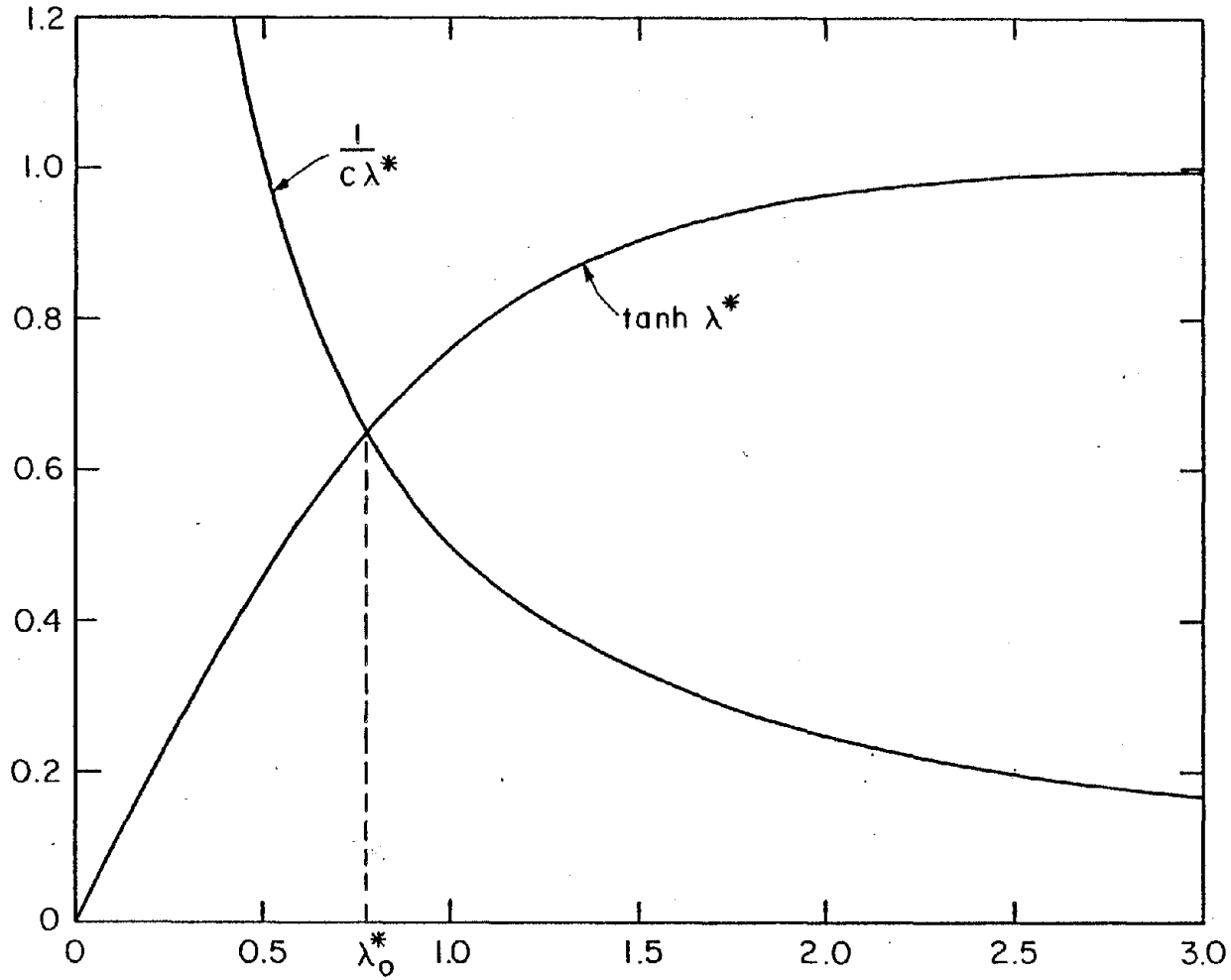

Figure 12. Diagram showing the method of finding the root of Eq. (2.14).

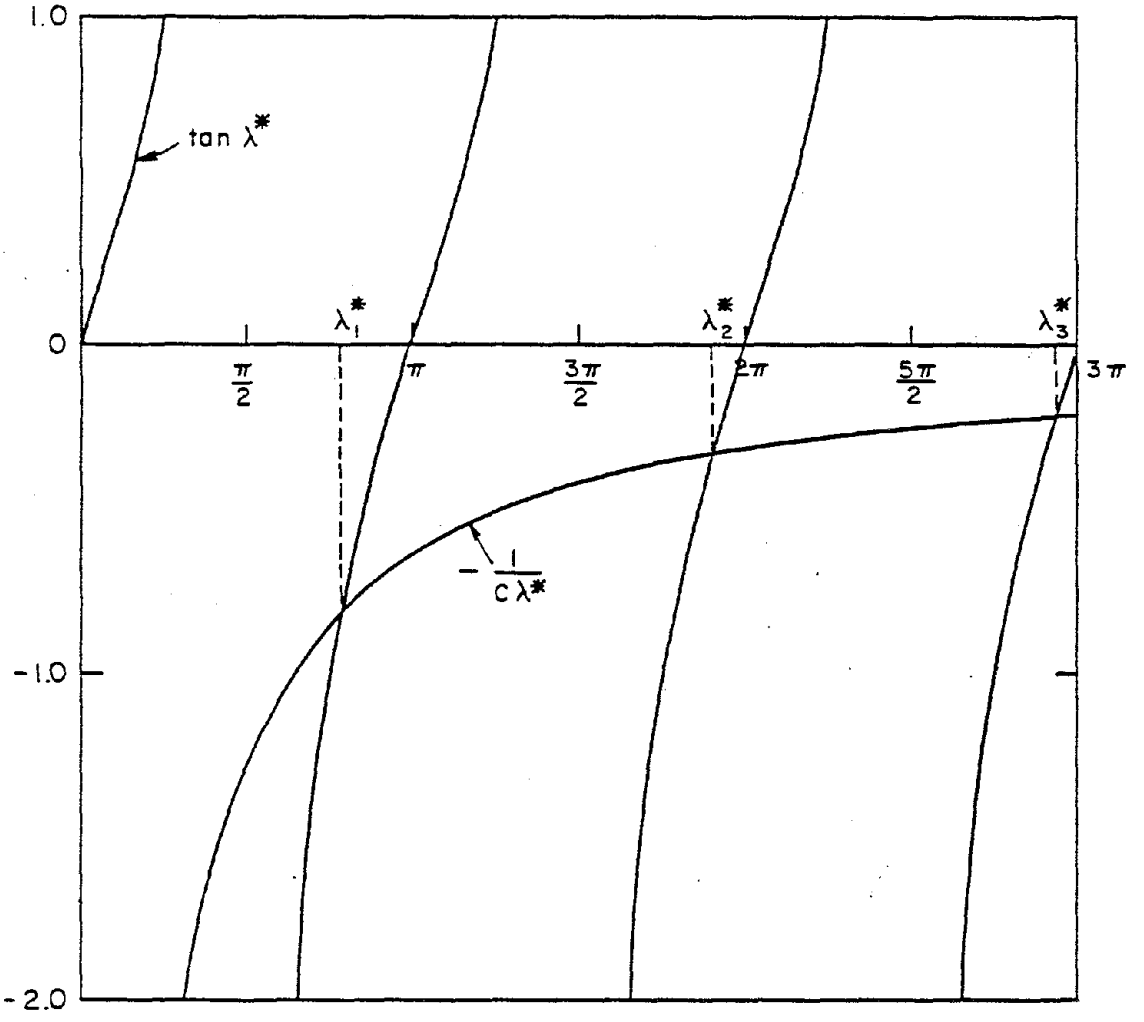

Figure 13. Diagram showing the method of finding the roots of Eq. (2.15).

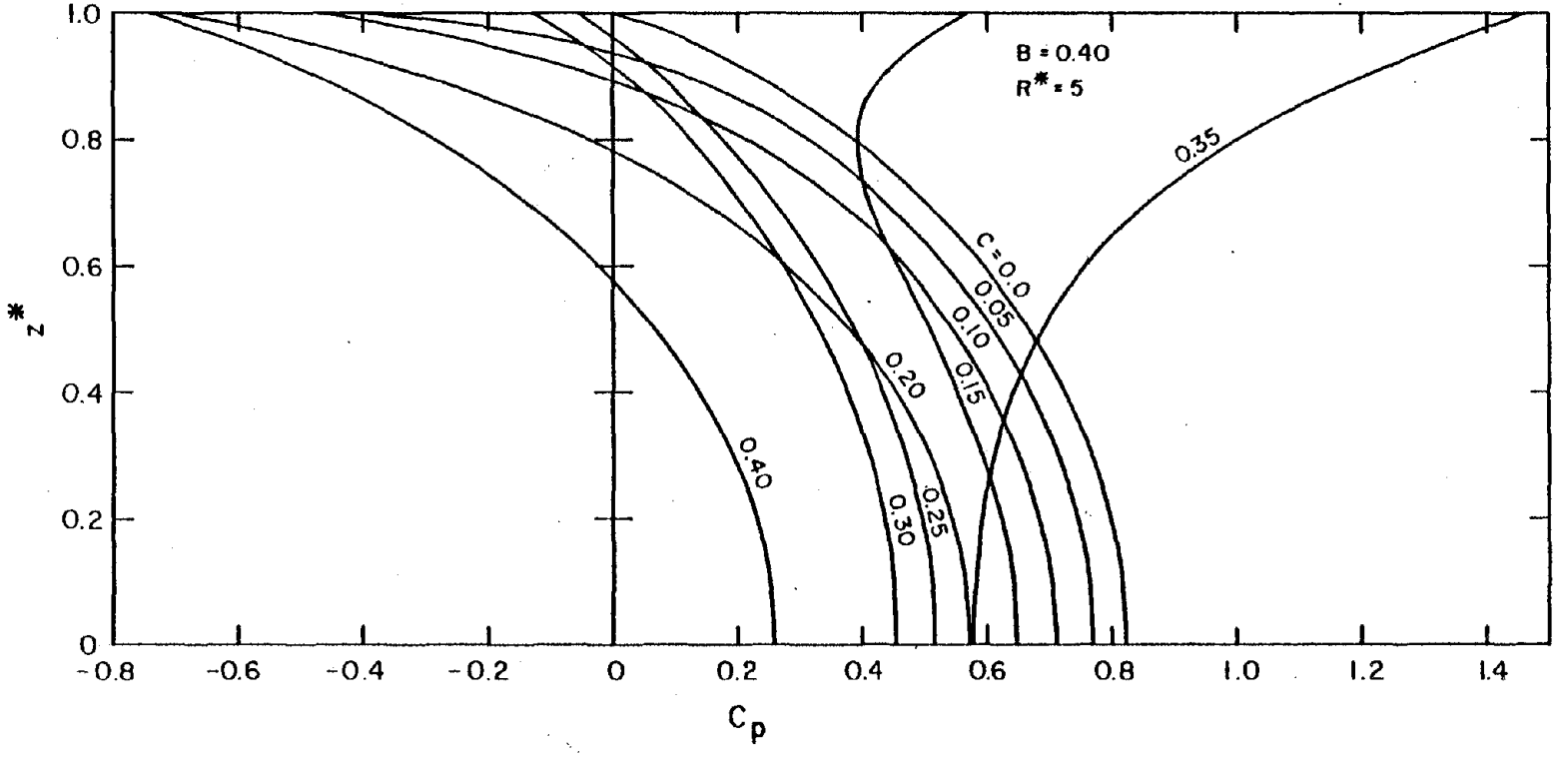

Figure 14. Variation of the pressure coefficient C_p with z*, for different values of the wave-effect parameter C. (Circular reservoir; B = 0.40, R* = 5.0).

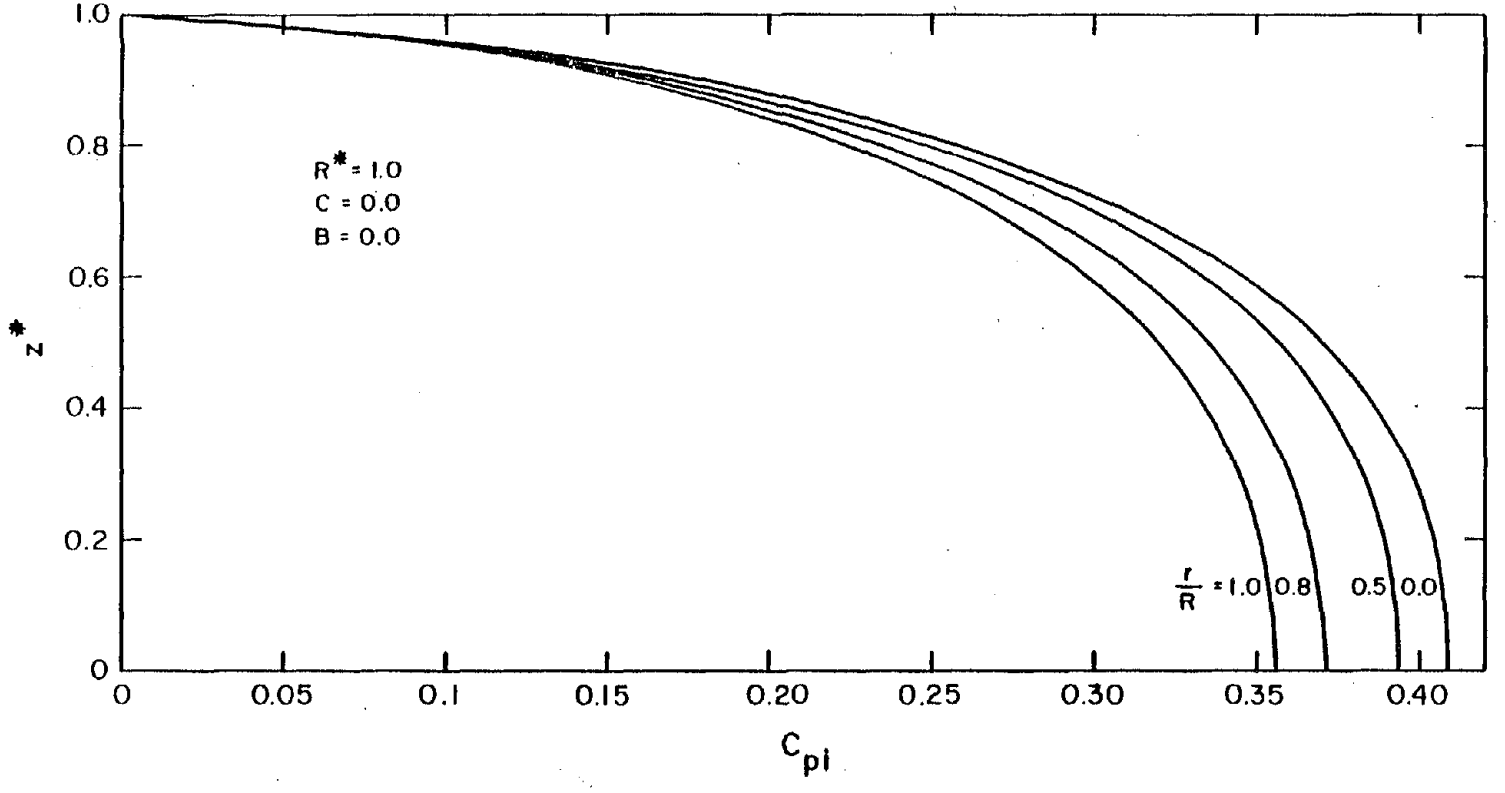

Figure 15. Variation of the in-phase pressure coefficient C_{pi} with z*, at different locations r/R. (Semi-circular reservoir; C = 0.0, B = 0.0, R* = 1.0).

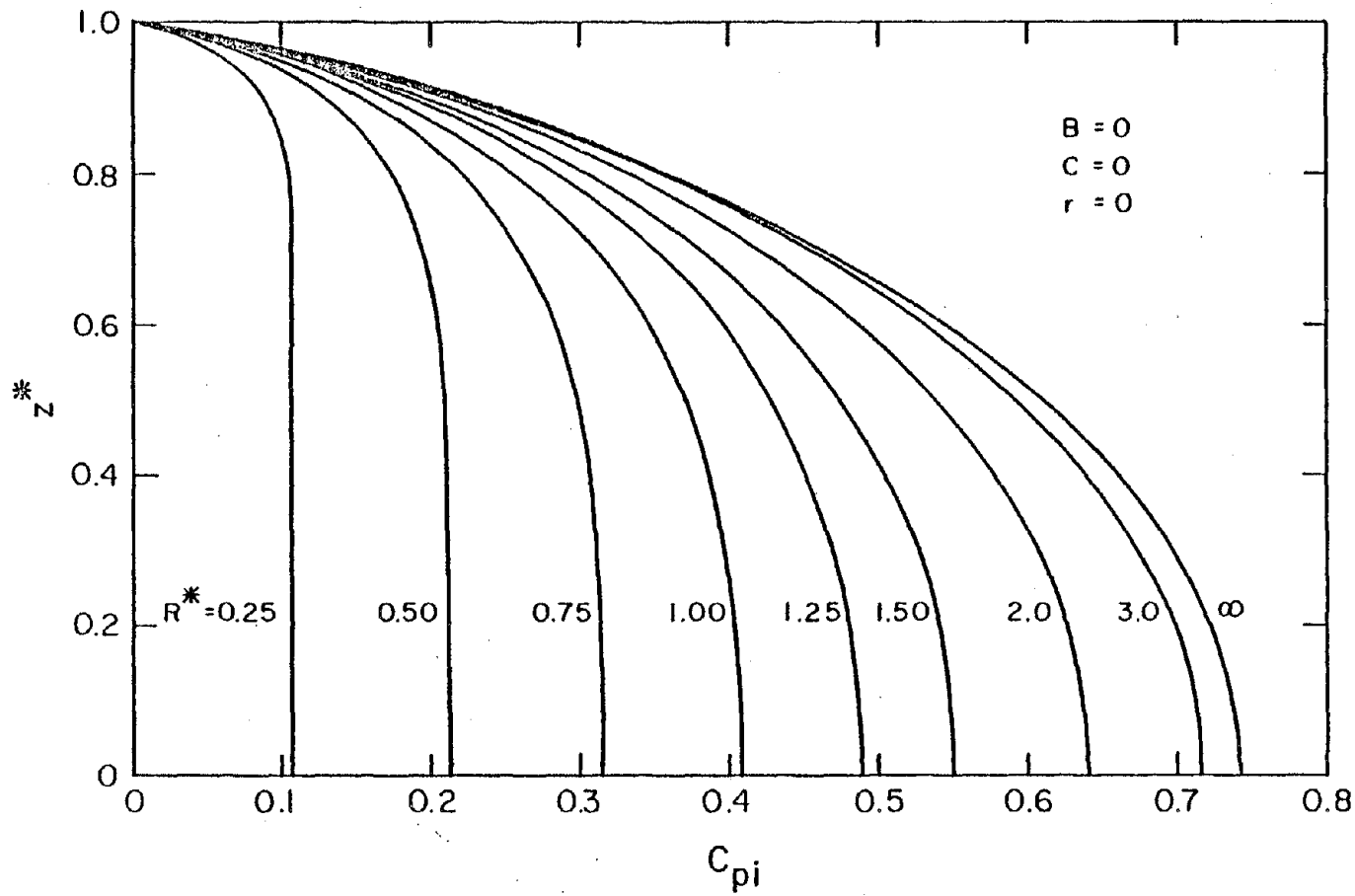

Figure 16. Variation of the pressure coefficient C_{pi} with z*, for different values of R*. (Semi-circular reservoir; C = 0.0, B = 0.0, r = 0).

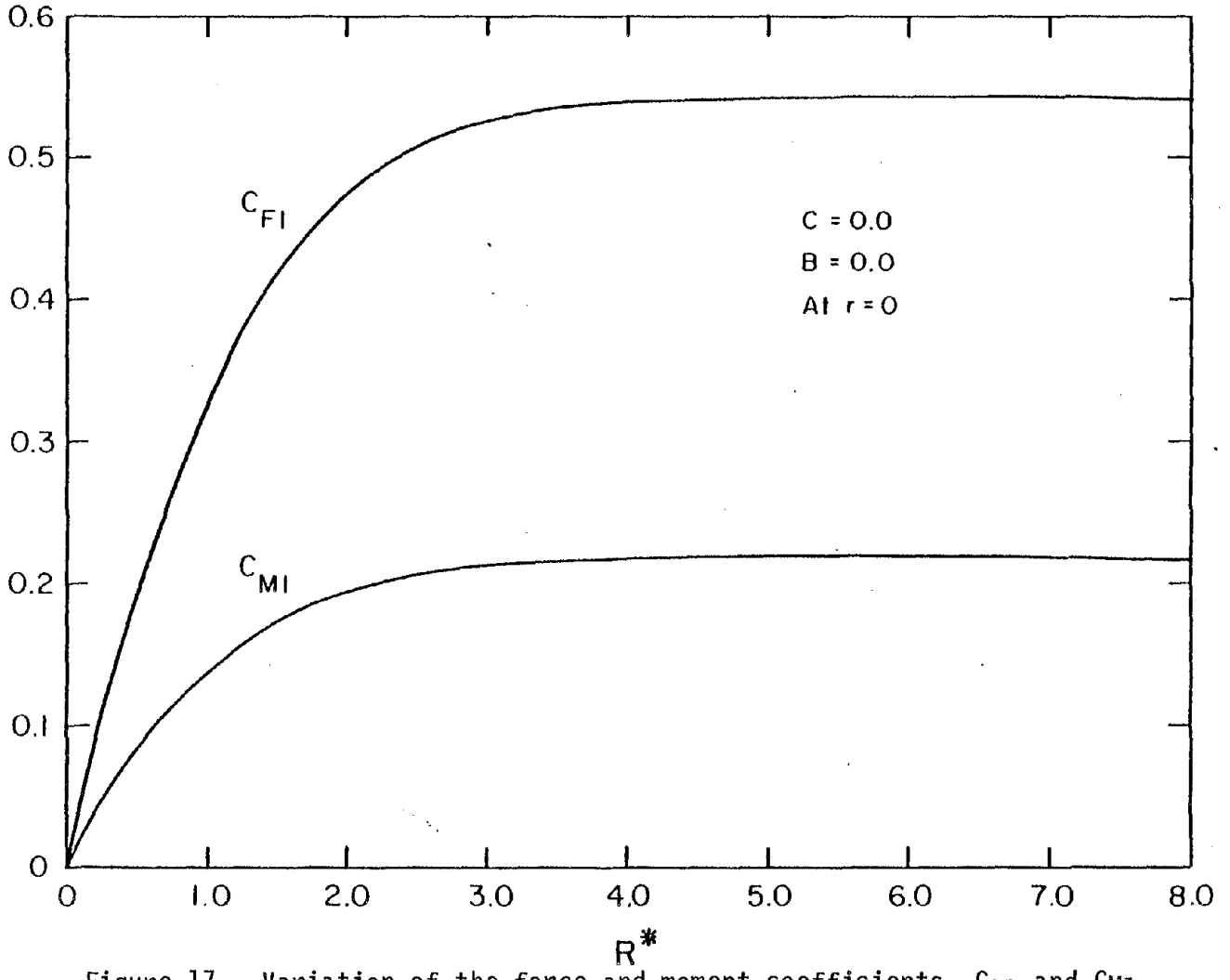

Figure 17. Variation of the force and moment coefficients, C_{FI} and C_{MI} respectively, with R*. (Semi-circular reservoir; C = 0.0, B = 0.0, r = 0).

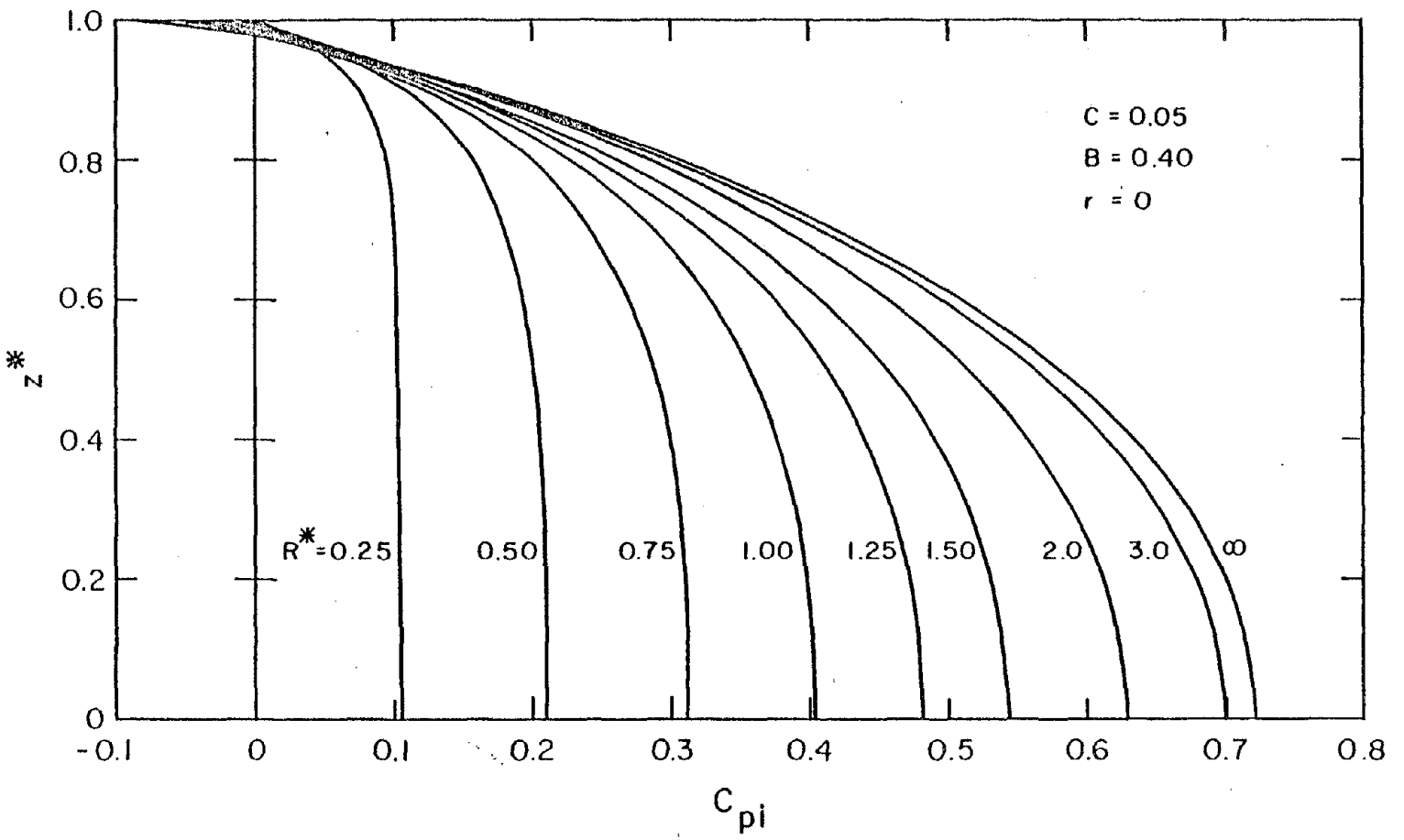

Figure 18. Variation of the pressure coefficient C_{pi} with z*, for different values of R*. (Semi-circular reservoir; C = 0.05, B = 0.40, r = 0).

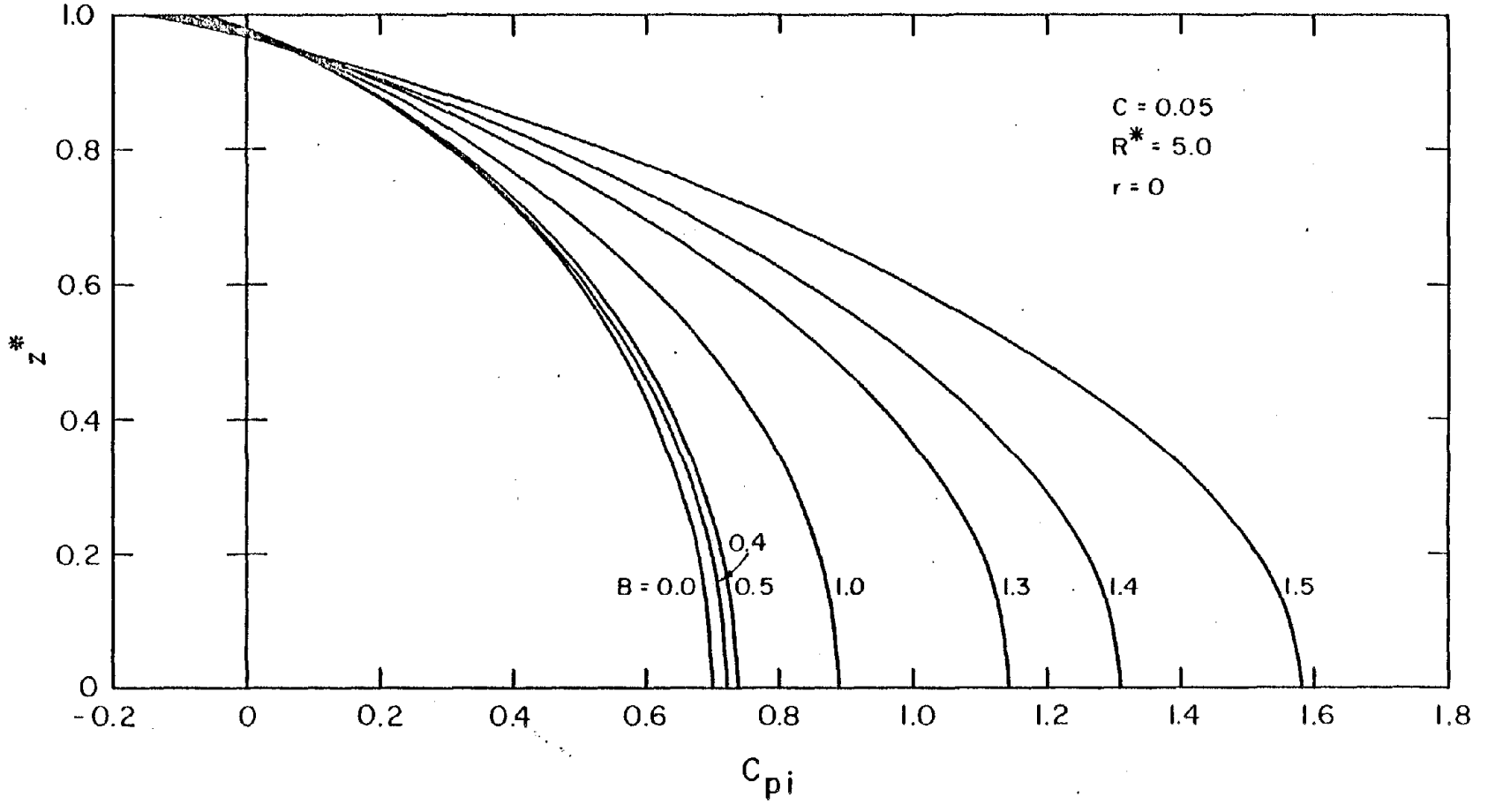

Figure 19. Variation of the pressure coefficient C_{pi} with z*, for different values of the compressibility parameter B. (Semi-circular reservoir; C = 0.05, R* = 5.0, r = 0).

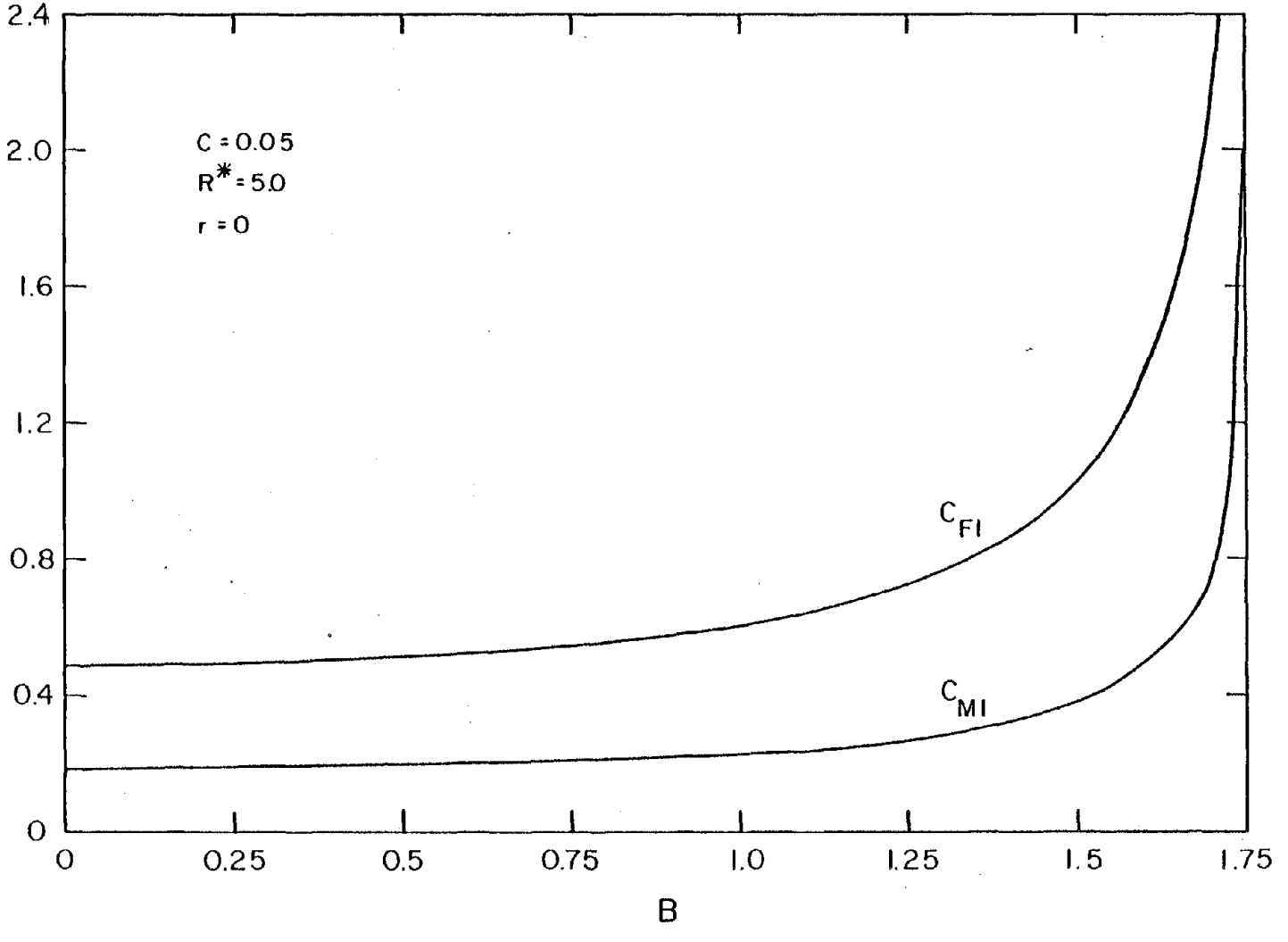

Figure 20. Variation of the force and moment coefficients, C_{FI} and C_{MI} respectively, with the compressibility parameter B. (Semi-circular reservoir; C = 0.05, R* = 5.0, r = 0).

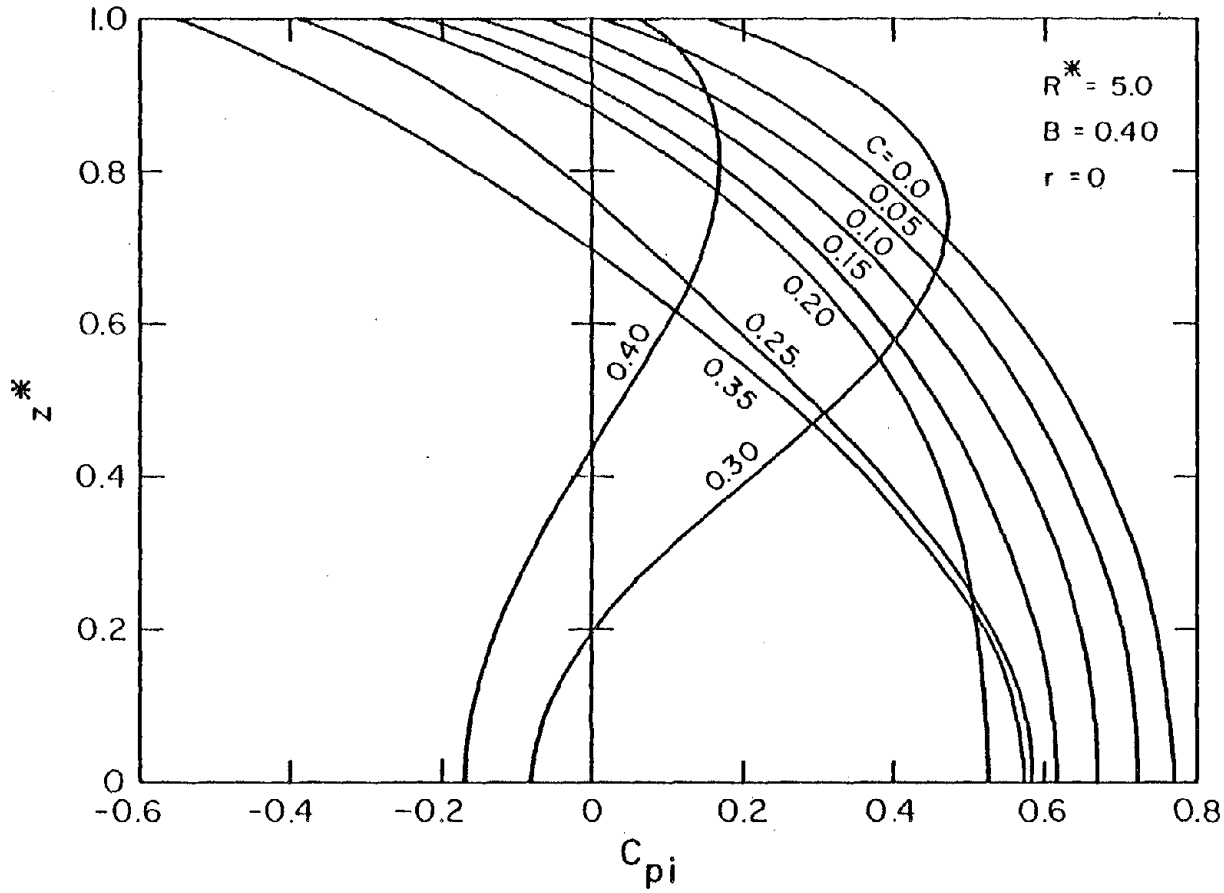

Figure 21. Variation of the pressure coefficient C_{pi} with z*, for different values of the wave-effect parameter C. (Semi-circular reservoir; B = 0.40, R* = 5.0, r = 0).